Albumin-STING Nanoagonist Reprograms HSPCs to Antitumor Neutrophils Enhancing MHC I–Mediated CD8$^+$ T Cell Immunity

Jinsong Tao[1, †], Hongyi Zhao[1, †], Chengyi Li[1], Hanning Wen[1], Fang Ke[1], Qiuxia Li[1], Miao He[1], Bo Wen[1], Zhongwei Liu[1], Wei Gao[1, 2, *], Duxin Sun[1, *]

[1] Department of Pharmaceutical Sciences, College of Pharmacy, Rogel Cancer Center, University of Michigan, Ann Arbor, MI 48109, USA

[2] Department of Pharmacology and Pharmaceutical Sciences, College of Pharmacy, University of Houston, TX, 77204, USA

[†] These authors contributed equally to this work

*Correspondence: wgao21@central.uh.edu (W.G.), duxins@umich.edu (D.S.)

Abstract

Tumor-associated immunosuppressive neutrophils, termed myeloid-derived suppressor cells (MDSCs), compromise cancer immunotherapy. They can be pathologically programmed as early the hematopoietic stem and progenitor cell (HSPC) stage by suppressing interferon signaling. Reprogramming HSPCs toward antitumor neutrophils through the stimulator of interferon genes (STING) activation offers a promising therapeutic strategy. Here, we demonstrate that an albumin-STING nanoagonist (Nano ZSA-51D) reprograms HSPCs to generate antitumor neutrophils, enhancing MHC I-mediated CD8$^+$ T cell immunity. Nano ZSA-51D activates STING–interferon signaling in HSPCs, promoting their expansion and differentiation toward granulocyte-monocyte progenitors via STING-NF-κB-IL-6 signaling. It further reprograms neutrophils into CD14$^+$ICAM-1$^+$ subset through STING-NF-κB–TNF-α signaling, enhancing tumor infiltration. These neutrophils upregulate interferon signaling and MHC I antigen presentation, boosting tumor-specific CD8$^+$ T cell responses. Adoptive transfer of Nano ZSA-51D-reprogrammed neutrophils with α-PD1 therapy achieves complete colon tumor remission. Our findings provide a novel strategy to reprogram HSPCs toward antitumor neutrophils and highlight the potential of early interventions at HSPC stage to rewire neutrophil fate for cancer immunotherapy.

INTRODUCTION

Tumor-associated immunosuppressive neutrophils, often referred to as myeloid-derived suppressor cells (MDSCs), are abundant in solid tumors that significantly compromise the efficacy of cancer immunotherapy in patients.[1,2] This heterogeneous population is pathologically programmed by cancer-derived signals for immunosuppression.[3,4] However, neutrophils can be programmed into either antitumor (N1) or protumor (N2) subsets.[5-7] For instance, high neutrophil infiltration in tumors prior to immunotherapy is associated with poor prognosis, indicating an immunosuppressive role of neutrophils.[8,9] While neutrophil infiltration induced by immunotherapy is correlated with improved therapeutic outcomes, suggesting an antitumor function of neutrophils.[10-19] These antitumor neutrophils can directly kill tumor cells or act as antigen-presenting cells (APCs) to active T cell responses, thereby sensitizing tumors to anti-PD1 (α-PD1) therapy.[16-19]

Previous approaches have primarily focused on reprogramming neutrophils within the tumor microenvironment (TME) to reverse their immunosuppressive functions. Recent studies discover that the antitumor (N1) or protumor (N2) neutrophils may be programmed as early as the hematopoietic stem and progenitor cell (HSPC) stage, rather than solely through interconversion within the TME, due to the short lifespan of mature neutrophils.[20-25] For example, tumor-derived signals can imprint immunosuppressive programming onto HSPCs, leading to the development of pro-tumor neutrophils.[20-22] Conversely, certain immune interventions using Mycobacterium bovis Bacillus Calmette-Guérin (BCG) have been shown to reprogram HSPCs toward antitumor myeloid cells, including neutrophils and monocytes, that overcome tumor-induced immunosuppression.[23] These findings highlight the therapeutic potential of reprogramming HSPCs toward antitumor neutrophils before exposure to cancer-derived signals.

Emerging evidence suggests that cancer-derived signals suppress the interferon response in granulocyte-monocyte progenitors (GMPs), reprogramming their differentiation toward immunosuppressive MDSC.[25] The downregulation of interferon signaling is a key driver of their immunosuppressive phenotype.[26,27] In contrast, interferon-stimulated neutrophils exhibit potent antitumor activity to sensitize α-PD1 immunotherapy in both mice and humans.[10,16] Therefore, we aim to activate the stimulator of interferon genes (STING) pathway to restore the interferon signaling in both HSPCs and MDSCs. The STING pathway activation triggers phosphorylation of

59 TBK1–IRF3 and NF-κB to induce interferons and proinflammatory cytokines such as TNF-a and
60 IL-6, thereby promoting immunity.[28-30] Notably, STING expression is higher in HSPCs than in
61 their differentiated immune progeny, suggesting a unique function in early lineage
62 programming.[31,32] We hypothesize that STING agonist could activate interferon signaling in
63 HSPCs and reprogram them toward antitumor neutrophils, thereby reversing tumor-driven MDSC
64 development. Moreover, how STING activation reprograms HSPCs to antitumor neutrophils and
65 the underlying antitumor mechanisms of these neutrophils for cancer immunotherapy remain
66 elucidated.

67 Here, we developed an albumin-STING nanoagonist (Nano ZSA-51D) that reprograms HSPCs to
68 antitumor neutrophils with enhanced MHC I antigen presentation, which migrate from bone
69 marrow into tumors to remodel the TME and promote $CD8^+$ T cell immunity (**Fig. 1a**). The dimeric
70 STING agonist ZSA-51D was synthesized from our monomeric STING agonist ZSA-51[33] and
71 encapsulated into mouse albumin to generate Nano ZSA-51D. Nano ZSA-51D activated the
72 STING–interferon signaling in HSPCs, promoting their expansion and skewing differentiation
73 toward GMPs through STING-NF-κB-IL-6 signaling in bone marrow. It further reprogrammed
74 immature ($CD101^-$) and mature ($CD101^+$) neutrophils into $CD14^+ICAM\text{-}1^+$ subsets through
75 STING–NF-κB–TNF-α signaling, thereby enhancing tumor infiltration. Transcriptomic and
76 immune profiling revealed that these neutrophils upregulated interferon signaling and MHC I
77 antigen presentation to boost tumor-specific $CD8^+$ T cell responses. Importantly, adoptive transfer
78 of Nano ZSA-51D-reprogrammed neutrophils in combination with α-PD1 therapy achieved
79 complete remission of colon tumors with durable immune memory. Nano ZSA-51D combined
80 with α-PD1 exhibited potent efficacy in colon cancer and pancreatic cancer models.

81 **RESULTS**

82 **Albumin-STING Nanoagonist (Nano ZSA-51D) Potently Activates STING Signaling**
83 **Pathway and Enhances Bone Marrow Delivery**

84 Building on our previously developed monomeric STING agonist, ZSA-51,[33] we synthesized a
85 novel non-CDN dimeric STING agonist, ZSA-51D, which exhibited superior STING pathway
86 activation (**Fig. 1a, Left**). ZSA-51D is an ester-based prodrug, that requires hydrolysis by esterases
87 to convert into its active acid form (ZSA-52D) before binding to STING protein. Both ZSA-51D
88 and ZSA-52D were synthesized (**Fig. S1**). Due to its enhanced cell permeability, ZSA-51D can be

easily uptake inside cells and efficiently converted to ZSA-52D, resulting in potent and sustained STING activation. As anticipated, ZSA-51D showed no binding with human STING, whereas the activated form ZSA-52D displayed a potent binding affinity to human STING, with an IC_{50} of 1.17 nM (**Fig. 1b**). In THP1-Blue™ ISG reporter cells, ZSA-51D demonstrated a superior EC_{50} of 5.1 nM, outperforming ZSA-52D (EC_{50} = 14.1 nM) and monomer ZSA-51 (EC_{50} = 52.6 nM) (**Fig. 1c**).

To facilitate systemically intravenous administration, we encapsulated ZSA-51D into an albumin nanoparticle (Nano ZSA-51D).[34-36] The average particle size of Nano ZSA-51D was 100.2 ± 4.3 nm (**Fig. 1d**). Notably, Nano ZSA-51D exhibited an 11.6-fold enhancement in STING activation (EC_{50} = 0.44 nM) compared to free ZSA-51D (EC_{50} = 5.1 nM) in THP1-Blue™ ISG cells (**Fig. 1e**). The pharmacokinetics studies showed that Nano ZSA-51D enhanced bone marrow accumulation compared to free ZSA-51D (**Fig. 1f**), whereas drug distribution in tumor and systemic circulation was similar between the two groups (**Fig. S2**). Western blot analysis further confirmed that Nano ZSA-51D significantly enhanced phosphorylation of STING and downstream effectors IRF3 and NF-κB p65 in bone marrow cells**,** thereby promoting the production of IFN-β, TNF-α and IL-6 (**Fig. S3**).[30] These results indicate that Nano ZSA-51D potently activates both the STING-IRF3 and STING-NF-κB pathways.

Nano ZSA-51D Expands HSPCs and Skews Differentiation Toward GMPs

Neutrophils are derived from HSPCs in the bone marrow through a series of progressively restrictive differentiation steps (**Fig. S4A**). To further explore whether Nano ZSA-51D–mediated STING activation effects on HSPCs in vivo, we analyzed the composition of HSPC subsets in bone marrow of MC-38 colon tumor-bearing mice 24 hours after 3 doses (1 mg/kg, I.V.) (**Fig. 1g**).

Surprisingly, both free and Nano ZSA-51D treatments resulted in a marked expansion of the HSPCs ($Lin^{-}Sca\text{-}1^{+}c\text{-}Kit^{+}$, LSK) (**Fig. 1h**), which includes long-term hematopoietic stem cell (LT-HSC), short-term HSC (ST-HSC) and multipotent progenitor (MPP) (**Fig. 1i and Fig. S4B**).[37] Notably, MPP exhibited the most dramatic expansion, rising from 4.1% to 25.3%. Among the MPP, the myeloid-biased multipotent progenitor 3 (MPP3) highly increased, while the lymphoid-biased multipotent progenitor 4 (MPP4) decreased, respectively (**Fig. 1j and Fig. S4C**). In downstream progenitors, we also observed an increase in granulocyte-monocyte progenitor (GMP) (**Fig. 1k and Fig. S4D**). These results suggest that Nano ZSA-51D expands HSPCs and skews

differentiation toward granulocyte-monocyte progenitors (GMP), thereby potentially enhancing myeloid lineage output and supporting innate immune responses (**Fig. 1l**).

Nano ZSA-51D Expands HSPCs and Skews Differentiation Toward GMP via STING-NF-κB-IL-6 Signaling

To elucidate how STING agonists can expand HSPCs and skew differentiation toward GMP, we isolated the HSPCs (LSK cells) from the bone marrow of MC-38 tumor-bearing C57BL/6J mice and treated them with Nano ZSA-51D (100 nM) for 3 days in vitro (**Fig. 1m**). Interestingly, Nano ZSA-51D dramatically expanded HSPCs (LSK populations) from 18.1% to 76.3% (**Fig. 1n**), while vehicle-treated groups exhibited the expected differentiation of HSPCs from LSK to LK populations. This observation suggests that STING activation can directly expand HSPCs at stem and multipotent progenitor states.

Since STING activation can induce different downstream cytokines such as IFN-β, TNF-α, IFN-γ and IL-6, we further test which of these cytokines can expand the HSPCs and skew differentiation toward GMP. We treated the isolated HSPCs (LSK cells) with cytokines for 3 days and monitored the composition changes of HSPCs. Among these cytokines, only IL-6 significantly expanded HSPCs (LSK population) (**Fig. 1o and Fig. S5A)** and increased the GMP population (**Fig. 1p and Fig. S5B**). Given that IL-6 is a key downstream effector of the STING–NF-κB axis, these results suggest that Nano ZSA-51D initiates STING-NF-κB-IL-6 signaling to expand HSPCs, and skew differentiation toward the GMP.

Nano ZSA-51D Activates STING–Interferon Signaling in HSPCs

Cancer-derived signals can reprogram GMPs derived from HSPCs to promote immunosuppressive differentiation of MDSCs by suppressing interferon response.[25-27] To investigate whether Nano ZSA-51D activates the STING pathway to upregulate the interferon signaling in HSPCs, we performed mRNA sequencing on vehicle- and Nano ZSA-51D-treated HSPCs. Nano ZSA-51D significantly increased the expression of STING-induced cytokines, including IFN-β, TNF-α, IFN-γ and IL-6, and upregulated multiple interferon-stimulated genes, such as Irf1, Irf5, Irf7, Stat1, Stat2, Ifit1, and Isg15, among others (**Fig. 1r**). These results indicate that Nano ZSA-51D robustly activates the STING–interferon signaling in HSPCs, thereby reprogramming their transcriptional landscape toward an antitumor immune phenotype.

148 **Nano ZSA-51D Promotes Neutrophil Generation and Tumor Infiltration**

149 To determine whether Nano ZSA-51D–mediated HSPC expansion and GMP differentiation
150 promote neutrophil generation and tumor infiltration, we analyzed the neutrophils in bone marrow,
151 blood and tumors of MC-38 colon tumor-bearing mice 24 hours after 3 doses (1 mg/kg, I.V.) (**Fig.**
152 **S6A**).

153 In the bone marrow, both free and Nano ZSA-51D significantly increased proportion of neutrophils
154 among $CD45^+$ cells from 50.1% to 59.7% and 63.3%, respectively (**Fig. S6B**). In peripheral blood,
155 Nano ZSA-51D also elevated circulating neutrophils, but which was less than free ZSA-51D (**Fig.**
156 **S6C**). Interestingly, in MC-38 tumors, Nano ZSA-51D dramatically increased tumor-infiltrating
157 neutrophils from 11.2% to 56.7% of $CD45^+$ immune cells, a substantially greater increasement
158 than free ZSA-51D (**Fig. S6D**). Collectively, these results demonstrate that while both free and
159 Nano ZSA-51D promote granulopoiesis to generate neutrophils, Nano ZSA-51D more effectively
160 drives their infiltration into tumors.

161 **Nano ZSA-51D Reprograms Bone Marrow Neutrophils into $CD14^+ICAM\text{-}1^+$ Subset to**
162 **Enhance Tumor Infiltration**

163 Recent studies have demonstrated that the immature/activated ($CD101^-CD14^+$) subset of tumor-
164 infiltrating neutrophils is associated with improved responses to immunotherapy.[10,38-40] CD101 is
165 the maturation marker of neutrophils and CD14 is the activation marker of pattern recognition
166 receptor-mediated immune responses.[41-45] To understand how Nano ZSA-51D further reprograms
167 bone marrow neutrophils for tumor infiltration and antitumor activity, we analyzed neutrophil
168 subtypes in the bone marrow, peripheral blood, and tumors of MC-38 tumor-bearing mice 24
169 hours following STING agonist treatment.

170 In the bone marrow of vehicle-treated mice, most neutrophils were immature/inactivated
171 ($CD101^-CD14^-$). Nano ZSA-51D treatment lead a 4-fold increase in immature/activated ($CD101^-$
172 $CD14^+$) neutrophils from 7.5% to 29.6 %, which was higher than free ZSA-51D treatment (**Fig.**
173 **2a**).

174 In the blood circulation of vehicle-treated mice, most neutrophils were mature/inactivated
175 ($CD101^+CD14^-$) (**Fig. 2b)**. While Nano ZSA-51D treatment dramatically increased the
176 immature/activated ($CD101^-CD14^+$) neutrophils from 0.08% to 20%, and mature/activated

177 ($CD101^+CD14^+$) neutrophils from 9.1% to 47.2%, which were both substantially higher than free
178 ZSA-51D treatment. These data suggest that Nano ZSA-51D strongly activates both immature and
179 mature $CD14^+$ neutrophils, promoting their migration from bone marrow into bloodstream.

180 In the tumors, activated $CD14^+$ neutrophils preferentially infiltrated tumors following Nano ZSA-
181 51D treatment. Specifically, the proportion of immature/activated $CD101^-CD14^+$ neutrophils
182 increased from 2.0% to 11.2%, and mature/activated $CD101^+CD14^+$ neutrophils rose from 46.1%
183 to 66.8% (**Fig. 2c**). In contrast, although free ZSA-51D also expanded total neutrophil numbers in
184 bone marrow and blood (**Fig. S6**), it induced fewer $CD14^+$ subsets, resulting in less tumor
185 infiltration. In addition, Nano ZSA-51D induced $CD14^+$ neutrophils highly expressed intercellular
186 adhesion molecule-1 (ICAM-1, CD54) in bone marrow and blood circulation, which promote
187 $CD14^+$ICAM-1^+ neutrophil infiltration into tumor (**Fig. 2d-f** and **Fig. S7**).[46,47] These data suggest
188 that Nano ZSA-51D effectively reprograms immature ($CD101^-$) and mature ($CD101^+$) bone
189 marrow neutrophils into activated $CD14^+$ICAM-1^+ subsets that enhance infiltration into tumors.

190 **Nano ZSA-51D Reprograms Neutrophils into $CD14^+$ICAM-1^+ Subset through STING–NF-**
191 **κB–TNF-α Signaling**

192 To determine whether Nano ZSA-51D inducing $CD14^+$ICAM-1^+ neutrophils is mediated by
193 STING pathway activation, we isolated bone marrow cells from wild-type (WT) C57BL/6J and
194 STING knockout (C57BL/6J-Sting1gt/J) mice and treated them with free or Nano ZSA-51D (100
195 nM) in vitro for overnight. As expected, Nano ZSA-51D (100 nM) significantly increased both
196 $CD101^-CD14^+$ and $CD101^+CD14^+$ neutrophil populations with high ICAM-1 expression
197 ($CD14^+$ICAM-1^+) from WT C57BL/6J mice, exceeding the effects observed with free ZSA-51D
198 (**Fig. S8A, B**). However, bone marrow neutrophils from STING knockout mice failed to reprogram
199 neutrophiles into $CD101^-CD14^+$, $CD101^+CD14^+$ and $CD14^+$ICAM-1^+ neutrophil populations,
200 confirming the requirement of STING activation (**Fig. 2g, h and Fig. S8C, D**).

201 To further study which downstream mediators of STING signaling play a role in reprograming
202 neutrophil subtypes, we treated the isolated bone marrow neutrophils with TNF-α, IFN-β, IFN-γ
203 and IL-6. We also used TGF-β as a control for immunosuppressive signaling. Among these, only
204 TNF-α effectively reprogrammed bone marrow neutrophils into $CD101^-CD14^+$, $CD101^+CD14^+$
205 and $CD14^+$ICAM-1^+ subsets (**Fig. 2i and Fig. S9A-D**). After TNF-α neutralization with antibody
206 treatment, Nano ZSA-51D no longer reprogrammed neutrophils into the $CD14^+$ICAM-1^+ subset

207 (**Fig. 2j and Fig. S9E**). Given that TNF-α is a key effector of STING-NF-κB axis, these findings
208 suggest that Nano ZSA-51D reprograms immature and mature bone marrow neutrophils into
209 $CD14^+$ICAM-1^+ subsets via STING-NF-κB-TNF-α signaling, enabling their infiltration into
210 tumors (**Fig. 2k**).

211 **Nano ZSA-51D-Reprogrammed Neutrophils Drive Complete MC-38 Tumor Remission with**
212 **α-PD1 Therapy**

213 To determine whether Nano ZSA-51D-reprogrammed bone marrow neutrophils possess antitumor
214 activity, we isolated three neutrophil subsets from bone marrow cells treated with Nano ZSA-51D
215 (100 nM) in vitro: immature/inactivated ($CD101^-CD14^-$), immature/activated ($CD101^-CD14^+$)
216 and mature/activated ($CD101^+CD14^+$). Each subset was adoptively transferred intratumorally (I.T.)
217 into MC-38 tumors in combination with α-PD1 therapy (**Fig. 2l**).

218 Interestingly, adoptive transfer of immature/activated ($CD101^-CD14^+$) neutrophils combined with
219 α-PD1 achieved 100% tumor complete remission (100% CR) without recurrence, resulting in 100%
220 long-term survival (**Fig. 2m, n and Fig. S10**). The mature/activated ($CD101^+CD14^+$) neutrophils
221 also significantly enhanced anti-tumor efficacy, achieving a 60% CR rate. In contrast, the
222 immature/inactivated ($CD101^-CD14^-$) neutrophils with α-PD1 did not significantly improve
223 therapeutic outcomes compared to α-PD1 monotherapy. These findings suggest that Nano ZSA-
224 51D-reprogrammed $CD14^+$ neutrophils possess potent antitumor properties that synergize with α-
225 PD1 therapy.

226 To investigate whether the anti-tumor effect conferred by $CD101^-CD14^+$ neutrophils involved
227 long-term immune memory, mice that achieved complete remission were rechallenged with MC-
228 38 tumor cells 120 days post-treatment (**Fig. S11A**). Notably, these mice completely resisted tumor
229 re-growth (**Fig. S11B**), indicating the establishment of durable antitumor immune memory.

230 To further characterize the immune memory response, we analyzed $CD8^+$ and $CD4^+$ T cell memory
231 subsets in the spleen, lymph nodes and blood of cured MC-38 mice at 180-day post-rechallenge
232 (**Fig. S11A**). Flow cytometry analysis revealed a significant increase in $CD8^+$ T central memory
233 (TCM) cells in cured MC-38 mice, with a 1.53-, 2.40- and 1.84-fold increase in spleen, lymph
234 nodes and blood compared to naïve mice (**Fig. S11C, E, F**). $CD4^+$ T effector memory (TEM) cells
235 also increased in all tissues examined, while $CD4^+$ TCM cells remained unchanged (**Fig. S11D, F,**

236 **H**). These results demonstrate that adoptive transfer of $CD101^{-}CD14^{+}$ neutrophils with α-PD1
237 therapy promotes long-term $CD8^{+}$ T cell memory, driving complete tumor remission and long-
238 lasting tumor immunity.

239 **Nano ZSA-51D Upregulates Interferon Signaling and MHC I Antigen Presentation in**
240 **Neutrophils**

241 To further elucidate how Nano ZSA-51D-reprogrmmed neutrophils contribute to anticancer
242 efficacy, we performed bulk mRNA sequencing on sorted total neutrophils and their subtypes from
243 bone marrow cells following Nano ZSA-51D (100 nM) treatment in vitro. Differential gene
244 expression analysis revealed that antitumor neutrophil (N1) markers were upregulated, while
245 protumor (N2) markers were downregulated following treatment, indicating a shift toward an N1-
246 like neutrophil phenotype[48-50] (**Fig. 3a**).

247 Moreover, the interferon-stimulated genes (ISGs) were highly upregulated in neutrophils
248 following Nano ZSA-51D treatment (**Fig. 3b**). GO Gene set enrichment analysis (GSEA) further
249 revealed significant enrichment of the gene response to IFN-β (NES = 2.83, FDR q = 2.23E-21)
250 in Nano ZSA-51D treated neutrophils (**Fig. 3c**), indicating that STING pathway activation drives
251 IFN-β–mediated interferon signaling in these cells.

252 KEGG pathway enrichment analysis identified the top 20 hallmark pathways altered in neutrophils
253 by Nano ZSA-51D (**Fig. 3d**). Among them, the key innate immune signaling pathways were highly
254 enriched and upregulated, including Cytosolic DNA-sensing, NOD-like receptor, toll-like receptor
255 and C-type lectin receptor pathways, along with their downstream signaling cascades such as the
256 TNF and NF-kappa B pathways (**Fig. 3e and Fig. S12A, B**). These pathways play critical roles in
257 enabling the $CD14^{+}$ neutrophils to detect pathogen-associated molecular patterns (PAMPs) and
258 damage-associated molecular patterns (DAMPs) in the TME.[51-54]

259 A striking finding was the significant enrichment and upregulation of antigen processing and
260 presentation pathway (NES = 2.00, FDR q = 4.36E-5) in neutrophils by Nano ZSA-51D treatment,
261 as well as immature/activated ($CD101^{-}CD14^{+}$) (NES = 2.03, FDR q = 3.49E-5) and
262 mature/activated ($CD101^{+}CD14^{+}$) (NES = 2.1, FDR q = 2.24E-6) neutrophils (**Fig. 3d, e and Fig.**
263 **S12C)**. Further GO GSEA analysis confirmed that MHC class I-mediated antigen processing and
264 presentation were highly upregulated in $CD101^{-}CD14^{+}$ and $CD101^{+}CD14^{+}$ neutrophils (**Fig. 3f,**

265 **g)**. In contrast, MHC class II-mediated antigen processing and presentation remained unchanged
266 (NES < 1.5, FDR q > 0.05).

267 Consistently, Nano ZSA-51D markedly upregulated the expression of MHC class I subunits,
268 costimulatory ligands, T cell-activating cytokines and T cell-recruiting chemokines in these
269 neutrophils, further reinforcing their antigen-presenting potential **(Fig. 3h)**. In contrast, MHC class
270 II subunit expression remained unchanged **(Fig. S12F**).

271 To verify MHC class I antigen presentation by Nano ZSA-51D-reprogrammed neutrophils, we
272 performed flow cytometry analysis on bone marrow neutrophils treated with Nano ZSA-51D and
273 OT-I peptide (CSSSIINFEKL from OVA). Nano ZSA-51D significantly upregulated MHC class I
274 expression on neutrophils (**Fig. 3i**), while MHC class II expression remained unchanged (**Fig. 3j**).
275 Importantly, MHC class I presentation of OT-I peptide (H-2K^b OT-I complex) was greatly
276 enhanced 3.6-fold on neutrophils after Nano ZSA-51D treatment (**Fig. 3k**). Both
277 immature/activated (CD101$^-$CD14$^+$) and mature/activated (CD101$^+$CD14$^+$) neutrophils
278 demonstrated superior antigen presenting capacity compared to vehicle-treated control (**Fig. 3l**).
279 These results suggest that Nano ZSA-51D reprograms neutrophils with enhanced MHC I antigen-
280 presentation capacity, potentially enabling effective priming of CD8$^+$ T cell immunity (**Fig. 3m**).

281 **Nano ZSA-51D-Reprogrammed Neutrophils Primes Antigen-Specific CD8$^+$ T Cell Responses**

282 To investigate whether Nano ZSA-51D-reprogrammed neutrophils can effectively prime antigen-
283 specific CD8$^+$ T cell activation and proliferation via MHC I-mediated antigen presentation, we
284 conducted a co-culture experiment using OT-I CD8$^+$ T cells from transgenic OT-I mice. We sorted
285 total neutrophils from bone marrow cells that pre-treated with ovalbumin (OVA, 0.2 mg/mL) and
286 Nano ZSA-51D (100 nM), and co-incubated them with OT-I CD8$^+$ T cells for 48 hours (**Fig. 4a**).

287 Strikingly, neutrophils treated with OVA and Nano ZSA-51D induced extensive OT-I CD8$^+$ T cell
288 clustering (**Fig. 4b**), suggesting enhanced recruitment, activation, and proliferation of OT-I CD8$^+$
289 T cells. Flow cytometry analysis further confirmed that OVA and Nano ZSA-51D co-treated
290 neutrophils strongly activated OT-I CD8$^+$ T cells, as indicated by a significant increase in CD69,
291 CD25 and CD137 (4-1BB) expression (**Fig. 4c and Fig. S13A, B**). Moreover, they significantly
292 promoted the proliferation of OT-I CD8$^+$ T cells, as demonstrated by flow cytometry proliferation

293 assays (**Fig. 4d**). These data suggest Nano ZSA-51D-reprogrammed neutrophils activate $CD8^+$ T
294 cell responses through enhanced MHC I antigen presentation.

295 To further assess the $CD8^+$ T cell activation potential of immature and mature $CD14^+$ neutrophils,
296 we sorted these two distinct neutrophil subtypes from bone marrow cells that were treated with
297 OVA and Nano ZSA-51D, and co-incubated them with OT-I $CD8^+$ T cells for 48 hours. Both
298 immature/activated ($CD101^-CD14^+$) and mature/activated ($CD101^+CD14^+$) neutrophils treated
299 with OVA and Nano ZSA-51D induced prominent OT-I $CD8^+$ T cell clustering (**Fig. 4e**). Further
300 Flow cytometry analysis revealed that both $CD101^-CD14^+$ and $CD101^+CD14^+$ neutrophils strongly
301 activated OT-I $CD8^+$ T cells, as indicated by increased expression of CD69, CD25, and CD137 (4-
302 1BB) (**Fig. 4f and Fig. S13C, D**) and significantly promoted OT-I $CD8^+$ T cell proliferation (**Fig.**
303 **4g**). These results demonstrated that Nano ZSA-51D-reprogrammed immature and mature $CD14^+$
304 neutrophils mediated potent antigen-specific $CD8^+$ T cell activation and proliferation.

305 **Nano ZSA-51D in Combination with α-PD1 Achieved Potent Therapeutic Efficacy in Colon**
306 **and Pancreatic Cancer Models**

307 Next, we evaluated the antitumor efficacy of Nano ZSA-51D in both MC-38 colon cancer and
308 pancreatic cancer model (**Fig. 5a**). Notably, Nano ZSA-51D (1 mg/kg, I.V.) in combination with
309 α-PD1 (100 μg/mice) achieved 100% tumor complete remission (100% CR) without recurrence,
310 leading to 100% long-term survival (**Fig. 5b, c, Fig. S14**). By comparison, free ZSA-51D with α-
311 PD1 significantly inhibited tumor growth with 80% CR, while clinically tested STING agonist
312 diABZI with 60% CR.

313 Furthermore, we evaluated the antitumor efficacy of Nano ZSA-51D in pancreatic ductal
314 adenocarcinoma (PDAC) which is not response to PD-1 therapy. We used KPC 6422 and KPC
315 6620 cell lines, derived from the KPC (Kras^G12D, p53^R172H, Pdx1-Cre) genetically
316 engineered mouse model of PDAC.[55] In both KPC 6422 and KPC 6620 pancreatic cancer models,
317 Nano ZSA-51D (1 mg/kg, I.V.) with/without α-PD1 significantly reduced tumor burden and extend
318 median survival, demonstrating superior efficacy over free ZSA-51D with/without α-PD1 (**Fig.**
319 **5d-g and Fig. S15, 16**). The Nano ZSA-51D at 2 mg/kg dose with α-PD1 led to significant tumor
320 remission and extended median survival by 3 weeks compared to PD-1 monotherapy (**Fig. 5f and**
321 **g**). In the KPC 6422 model, significant tumor shrinkage and scabbing were observed after the 4th
322 dose of Nano ZSA-51D (1 mg/kg, I.V.) with/without α-PD1 (**Fig. 5h**). In the 2 mg/kg Nano ZSA-

323 51D plus α-PD1 group, tumor scabbing occurred after the 2nd doses and completely disappeared
324 after the 4th dose, demonstrating rapid and effective tumor elimination.

325 **Nano ZSA-51D-Induced Neutrophil Infiltration Enhances Durable CD8$^+$ T Cell Responses**
326 **and Long-Term Memory in TME**

327 To further examine whether Nano ZSA-51D with/without α-PD1 therapy induces neutrophil
328 infiltration that enhances the CD8$^+$ T cell-mediated antitumor immune responses in TME, we
329 analyzed tumor-infiltrating neutrophils and T cells in MC-38 tumor-bearing mice by flow
330 cytometry at 1- and 4-day post-treatment (**Fig. 6a**).

331 At 1-day post-treatment, Nano ZSA-51D with α-PD1 dramatically increased tumor-infiltrating
332 neutrophils from 10.6% to 79.7% of CD45$^+$ immune cells, compared to vehicle-treated groups
333 (**Fig. 6b and Fig. S17A**), as well as the immature/activated (CD101$^-$CD14$^+$) neutrophils from 0.22%
334 to 13.5% (**Fig. 6c, e**), and the mature/activated (CD101$^+$CD14$^+$) neutrophils from 5% to 48.2%
335 (**Fig. 6d, e**). In contrast, free ZSA-51D with/without α-PD1 also slightly enhanced total neutrophils
336 and mature/activated (CD101$^+$CD14$^+$) neutrophils in tumors compared to vehicle-treated groups
337 but did not significantly increase immature/activated (CD101$^-$CD14$^+$) neutrophils (**Fig. 6c-e)**.
338 Conversely, 1-day post-treatment of Nano ZSA-51D with α-PD1 decreased macrophages from
339 59.7 % to 9.1 % of CD45$^+$ immune cells (**Fig. S17B, C**). A similar trend was observed in the KPC
340 6620 pancreatic cancer model, where 1-day post-treatment of Nano ZSA-51D with α-PD1
341 increased tumor-infiltrating neutrophils from 31.9% to 63.3% (**Fig. S18A, C**) and decreased
342 macrophages from 55.1% to 21.7% (**Fig. S18B, D**).

343 However, at 4-day post-treatment, tumor-infiltrating neutrophils declined compared to 1-day post-
344 treatment, with the most substantial reduction observed from 79.7% to 20.4% in the Nano ZSA-
345 51D with α-PD1 (**Fig. 6f and Fig. S19A**).

346 Concurrently, at 4-day post-treatment, Nano ZSA-51D with/without α-PD1 significantly increased
347 tumor-infiltrating CD3$^+$ T cells, with the most dramatic increase from 11.1% to 35.9% of CD45$^+$
348 immune cells in Nano ZSA-51D with α-PD1 group, which is significantly higher than that of free
349 ZSA-51D with/without α-PD1 (**Fig. 6g and Fig. S19B**). Further analysis revealed that Nano ZSA-
350 51D with/without α-PD1 expanded tumor-infiltrating CD8$^+$ T cells, while tumor-infiltrating CD4$^+$
351 T cell proportions remained unchanged among CD45$^+$ immune cells **(Fig. 6h-j)**. These results

352 suggested that Nano ZSA-51D-induced infiltration of immature and mature activated $CD14^+$
353 neutrophils enhances $CD8^+$ T cell responses in the TME.

354 To assess whether Nano ZSA-51D with α-PD1 therapy generates tumor-specific immune memory,
355 we performed tumor rechallenge experiments in cured MC-38 mice 100 days post-treatment (**Fig.**
356 **6k**). MC-38 tumor cells failed to establish tumors in Nano ZSA-51D with α-PD1 cured MC-38
357 mice, while KPC 6422 tumors grew at similar rates in both naïve and cured MC-38 mice (**Fig. 6l,**
358 **m**). These results suggest that Nano ZSA-51D with α-PD1 therapy induces a tumor-specific
359 immune memory response against MC-38 tumor cells but not against KPC 6422 tumor cells.

360 To further characterize the immune memory response, we also analyzed $CD8^+$ and $CD4^+$ T cell
361 memory subsets in the spleen, lymph nodes and blood of cured MC-38 mice 180 days after tumor
362 rechallenge (**Fig. 6k**). Flow cytometry analysis revealed a significant increase in $CD8^+$ T central
363 memory (TCM) cells in cured MC-38 mice, with a 3.3-, 4.4- and 4.5-fold increase in spleen, lymph
364 nodes and blood compared to naïve mice (**Fig. 6n and Fig. S20A, C**). While $CD4^+$ TCM cells had
365 no significant change (**Fig. 6o and Fig. S20B, D**). These results further confirm that Nano ZSA-
366 51D with α-PD1 therapy also generates the long term $CD8^+$ T cell memory, which contributes to
367 complete tumor remission and long-term tumor immunity.

368 **DISCUSSION**

369 Although the immunosuppressive role of MDSCs in cancer has been extensively studied over the
370 past decade, developing strategies to overcome neutrophil-mediated immune suppression remains
371 challenging.[1,2,7] Neutrophils exhibit remarkable plasticity and context-dependent functions,
372 rapidly adapting to tumor-derived signals, which complicates efforts to define their roles and
373 develop effective interventions against MDSC-mediated immune suppression.[3-6]

374 Recent evidence suggests that the immunosuppressive functions of MDSCs may be programmed
375 as early as the hematopoietic stem and progenitor cell (HSPC) stage by suppressing interferon
376 signaling.[20-25] Given that downregulated interferon signaling underlies MDSC-mediated
377 immunosuppression, we found that STING activation can activate STING-interferon signaling in
378 HSPCs and reprogram them toward antitumor neutrophils to enhance cancer immunotherapy. In
379 this study, we developed an albumin-STING nanoagonist (Nano ZSA-51D) that expanded HSPCs
380 and reprogrammed them to generate antitumor neutrophils with enhanced MHC I antigen

381 presentation, thereby activating $CD8^+$ T cell-mediated antitumor immunity. We further
382 demonstrated that Nano ZSA-51D combined with α-PD1 achieved potent anticancer efficacy in
383 colon and pancreatic cancer models.

384 While prior studies have mainly focused on STING-induced activation of dendritic cells and
385 macrophages, our work significantly broadens this paradigm by reprograming HSPCs to antitumor
386 neutrophils as key effector cells in STING-based immunotherapy. Our findings reveal that Nano
387 ZSA-51D expands HSPCs and skews their differentiation toward granulocyte-monocyte
388 progenitors (GMP) through STING–NF-κB–IL-6 signaling, eventually expanding the neutrophil
389 lineage. This suggests that STING signaling in the bone marrow is not merely an immune-sensing
390 pathway but also a potent regulator of hematopoietic fate of HSPCs. Mechanistically, STING
391 activation driven NF-κB-IL-6 signaling favors granulocyte-monocyte lineage commitment. Indeed,
392 IL-6 has been reported to drive HSPC proliferation and differentiation toward granulocyte-
393 monocyte progenitors that promote granulopoiesis, aligning with our observation.[56-58] In addition,
394 Nano ZSA-51D activates STING-interferon signaling in HSPCs and reprograms their
395 transcriptional landscape toward an antitumor immune phenotype, thereby promoting
396 differentiation into antitumor neutrophils rather than MDSCs. This finding suggests that early
397 STING activation at the progenitor level can reshape myelopoiesis, restoring immune surveillance
398 and preventing the pathological programming of immunosuppressive myeloid lineages by cancer-
399 derived signals.

400 Furthermore, this study reveals a previously underexplored antitumor role of neutrophils in
401 STING-mediated cancer immunotherapy.[59-61] We demonstrate that both immature ($CD101^-$) and
402 mature ($CD101^+$) bone marrow neutrophils are reprogrammed into $CD14^+ICAM\text{-}1^+$ subsets via
403 STING–NF-κB–TNF-α signaling by Nano ZSA-51D in bone marrow. These $CD14^+ICAM\text{-}1^+$
404 neutrophils infiltrate tumors more effectively and exhibit potent synergy with anti-PD1 therapy.
405 Notably, adoptive transfer of Nano ZSA-51D-reprogrmamed immature $CD14^+$ neutrophils in
406 combination with α-PD1 leads to 100% complete tumor remission through long-term $CD8^+$ T cell
407 central memory, highlighting their potent anti-tumor immune function. The upregulation of CD14
408 and ICAM-1 on neutrophils likely underlies these antitumor functions. CD14 acts as a co-receptor
409 for toll-like receptors, activating innate immunity responses to pathogens by binding PAMPs and
410 DAMPs.[44,62-64] While neutrophil ICAM-1 (CD54) expression is correlated with enhanced

411 migration, phagocytosis and costimulatory signal of T cell activation.[46,47,65-67] Studies also suggest
412 that ICAM-1 preferentially co-stimulates $CD8^+$ T cells while providing weak co-stimulation to
413 $CD4^+$ T cells.[68,69] Together, activation of CD14 and ICAM-1 on neutrophils may enhance their
414 responsiveness to PAMPs and DAMPs within the tumor microenvironment, promoting tumor
415 infiltration, antigen presentation, and activation of innate and adaptive immunity in synergy with
416 immune checkpoint blockade.

417 Transcriptomic and immune profiling reveal that Nano ZSA-51D-reprogrammed $CD14^+$
418 neutrophils upregulate interferon signaling and display high MHC class I levels, along with
419 enhanced costimulatory ligands and signaling. This confers them with enhanced MHC class I
420 antigen-presentation capacity, thereby supporting antigen-specific $CD8^+$ T cell-mediated
421 antitumor immunity. Previous studies also identified a subset of ICAM-$1^{hi}CD14^+$MHC I^{hi} APC-
422 like "hybrid neutrophils", derived from immature progenitors, that are capable of cross-presenting
423 antigens and initiating robust anti-tumor T cell responses in early-stage human lung cancer.[38,39,70]
424 In contrast, $CD11b^+CD14^-$ MDSCs have been shown to exert immunosuppressive effects on $CD8^+$
425 T cells, contributing to immune evasion in non-small cell lung cancer.[40] Collectively, these findings
426 suggest that Nano ZSA-51D induces $CD14^+$ICAM-1^+MHC I^{hi} neutrophils, acquiring antitumor
427 properties through enhanced MHC I-mediated antigen presentation to prime $CD8^+$ T cell responses.

428 Finally, despite extensive efforts to develop STING agonists that mimic natural cyclic dinucleotide
429 (CDNs), their clinical efficacy has remained limited.[71-73] CDN-based STING agonists suffer from
430 rapid enzymatic degradation and poor cellular permeability due to their hydrophilic and anionic
431 nature, restricting their use to intratumoral administration. To overcome these limitations,
432 nanoparticle-formulated CDNs and non-CDN STING agonists with improved pharmacological
433 properties have been developed for systemic bioavailability, demonstrating potent antitumor
434 activity.[33,73-77] Nevertheless, these non-CDN STING agonists may still have limited capacity to
435 reprogram HSPCs within the bone marrow and are often associated with toxicities. In contrast,
436 our albumin-STING nanoagonist, Nano ZSA-51D, exhibits unique anticancer efficacy by
437 reprogramming HSPCs into antitumor neutrophils in the bone marrow, while maintaining a
438 favorable safety profile. We evaluated the toxicity profile of Nano ZSA-51D by using single and
439 multiple doses (5 doses, 1 mg/kg, I.V.). Complete blood cell count, liver functions, and

440 histopathological assessments revealed no significant toxicity (**Fig. S21**), indicating that Nano
441 ZSA-51D is well tolerated.

442 In summary, we demonstrate that albumin-STING nanoagonist, Nano ZSA-51D, expands HSPCs
443 and reprograms them into antitumor neutrophils in the bone marrow, which subsequently migrate
444 into TME to enhance MHC I-mediated antigen presentation and activate $CD8^+$ T cell antitumor
445 immunity. Nano-ZSA51D combined with α-PD1 achieves potent anticancer efficacy in both colon
446 and pancreatic cancer models. These data suggest that Nano ZSA-51D provides a novel strategy
447 to reprogram HSPCs into antitumor neutrophils and highlight the potential of early interventions
448 at HSPC stage to rewire neutrophil fate for effective immunotherapy.

449 **MATERIALS AND METHODS**

450 **Cell cultures**

451 All cells were maintained at 37 °C in a humidified incubator (5% CO_2, 95% air). THP-1-Blue™
452 ISG cells (InvivoGen) were cultured in RPMI 1640 with 10% heat-inactivated FBS and 100 μg/ml
453 normocin. LSK cells from WT C57BL/6J mice were maintained in StemSpan medium with 50
454 ng/ml mouse SCF (BioLegend). Bone marrow neutrophils from WT and STING KO mice
455 (C57BL/6J-Sting1gt/J) and $CD8^+$ T cells from OT-I mice were cultured in RPMI 1640 with 10%
456 FBS. MC-38 colon adenocarcinoma cells (Kerafast) were cultured in DMEM with 10% FBS and
457 gentamycin. KPCY pancreatic cancer cells (KPC 6620 and KPC 6422; Kerafast) were cultured in
458 DMEM with GlutaMAX, 10% FBS, and sodium pyruvate. Unless otherwise indicated, all media
459 contained standard supplements (L-glutamine, HEPES, sodium pyruvate, nonessential amino acids,
460 and Pen/Strep). Key reagents and resources are listed in **Table S1**.

461 **Mice and tumor models**

462 All animal experiments were approved by the University of Michigan UCUCA and performed
463 under pathogen-free, temperature- and humidity-controlled conditions with a 12 h light/dark cycle.
464 WT C57BL/6J mice (Charles River), STING KO mice (C57BL/6J-Sting1gt/J), and OT-I
465 transgenic mice (C57BL/6-Tg(TcraTcrb)1100Mjb/J) (Jackson Laboratory) aged 6–8 weeks were
466 used. For tumor studies, 1×10^6 MC38, KPC 6620, or KPC 6422 cells in 100 μL FBS-free DMEM
467 were injected subcutaneously into the right flank of 6-week-old male WT mice. Mice were
468 randomized for treatment when tumors reached 50–100 mm^3 (day 6 post-inoculation), and tumor

growth and survival were monitored every 2–3 days. Tumor volume was calculated as length × width²/2.

Synthesis and characterization of dimeric STING agonist ZSA-51D

The dimeric STING agonist ZSA-51D were synthesized based on our previously reported monomeric STING agonist ZSA-51 (**Fig. S1**).[33,76] Briefly, starting material **1** was suspended in Et_2O and cooled to 0°C. MeMgBr was added to the suspension dropwise. The resulting mixture was stirred overnight to give intermediate **2**. **2** was stirred with PCC in DCM overnight to afford intermediate **3**. The solution of **3**, DIPEA and methyl thioglycolate in DMA was stirred at room temperature for 40 min under nitrogen atmosphere, followed by the addition of *t*-BuOK. The resulting mixture was heated at 80°C for 14 h to afford intermediate **4**. **4** was stirred with HATU, DCM, DIPEA and methyl 3-aminopropionate hydrochloride or *tert*-butyl 3-aminopropionate hydrochloride for 2 h at room temperature to provide intermediate **5a** or **5b**. **5a** or **5b** was deprotected under hydrogen atmosphere with palladium catalyst in ethanol to give intermediate **6a** or **6b**. **6a** or **6b** was dissolved in DCM. Then, TBDMSCl, imidazole and DMAP were added. The solution was stirred at room temperature for 0.5 h to give intermediate **7a** or 7**b**. The mixture of **7a** or **7b**, NBS, AIBN and CCl_4 was heated at 80°C for 2 h to produce intermediate **8a** or **8b**. **8a** or **8b** was suspended in CH_3CN and cooled to 0°C. Then, NMO was added. The mixture was stirred at room temperature overnight to give intermediate **9a** or **9b**. **9a** or **9b** was dissolved in DCM followed by the addition of PCC. The suspension was stirred at room temperature for 16 h to furnish intermediate **10a** or **10b**. TBAF (0.25 mL, 1 M in THF) was added into the solution of **10a** or **10b** in THF. The solution was stirred at room temperature for 0.5 h to afford intermediate **11a** or **11b**. The mixture of **11a** or **11b**, K_2CO_3, catalytic amount of NaI, CH_3CN and 1,3-dibromopropane was heated at 80°C for 3 h to produce intermediate **12a** or **12b**. **12a** or **12b** was mixed **11a** or **11b**, K_2CO_3, catalytic amount of NaI and CH_3CN, and heated at 80°C for 4 h to provide target compound ZSA-51D or intermediate **13b**. **13b** was dissolved in DCM followed by the addition of TFA. The solution was stirred at room temperature for 3 h to afford target compound ZSA-52D.

hSTING protein binding assay

The human STING WT binding assay (Revvity, PerkinElmer) was performed in white 386-well plates per the manufacturer's instructions. Test compounds (5 μL) were mixed with human STING

499 WT protein (5 μL, 6×His-tagged), followed by 10 μL of premixed d2 ligand and Tb cryptate-
500 conjugated antibody. Reactions were incubated at room temperature for 3 h, and HTRF signals
501 were measured using a Synergy 2 microplate reader (BioTek).

502 **THP1-Blue ISG cell assay**

503 THP1-Blue ISG cells (InvivoGen), a human monocytic line expressing a SEAP reporter under an
504 interferon-stimulated response element, were used to monitor IRF activation. Cells (1×10^6/mL)
505 were incubated with test compounds (100 μL) for 24 h at 37 °C. Supernatants (20 μL) were mixed
506 with 180 μL QUANTI-Blue™ reagent (InvivoGen) in 96-well plates and incubated for 2 h at 37 °C.
507 SEAP activity was measured at 620 nm using a Synergy 2 microplate reader (Biotek). All assays
508 were run in triplicate with vehicle controls.

509 **Nano ZSA-51D preparation**

510 Nano ZSA-51D was prepared as previously described.[35] Briefly, 10 mg ZSA-51D in 1 mL
511 chloroform was emulsified with 100 mg mouse serum albumin in 20 mL Milli-Q water using a
512 rotor-stator homogenizer. The emulsion was processed through six cycles at 20,000 psi with a
513 high-pressure homogenizer (4 °C), and chloroform was removed under reduced pressure at 25 °C.
514 The resulting suspension was lyophilized and stored at −20 °C. Particle size was measured by
515 dynamic light scattering (DLS; Zetasizer Nano-ZS, Malvern), with three measurements per sample
516 and experiments performed in triplicate.

517 **Western blot analysis of STING pathway activation**

518 Bone marrow cells from C57BL/6 mice were treated with vehicle, free, or Nano ZSA-51D (10 or
519 100 nM) for 4 h, lysed in RIPA buffer with protease and phosphatase inhibitors, sonicated, and
520 centrifuged at 12,000 × g for 15 min at 4 °C. Protein concentrations were determined by BCA
521 assay. Equal amounts of protein were separated by SDS-PAGE, transferred to PVDF membranes,
522 blocked with 5% milk in TBST, and incubated with primary antibodies against STING, p-STING
523 (Ser365), IRF3, p-IRF3 (Ser396), NF-κB p65, and p-NF-κB p65 (Ser536), followed by HRP-
524 conjugated secondary antibodies. Signals were detected using ECL (Bio-Rad) and imaged with a
525 ChemiDoc MP system.

526 **Cytokine secretion assay**

527 Bone marrow cells were treated with vehicle, free ZSA-51D, or Nano ZSA-51D (100 nM) for 48
528 h. Supernatants were collected, and IFN-β, TNF-α, and IL-6 levels were quantified using mouse-
529 specific ELISA kits (R&D Systems) per the manufacturer's instructions. Absorbance was
530 measured at 450 nm (Synergy 2, Biotek), and cytokine concentrations were calculated from
531 standard curves.

532 **In vivo treatment regimen**

533 Mice were intravenously administered free or Nano ZSA-51D (1 mg/kg), free diABZI (1 mg/kg),
534 or vehicle (15 mg/kg mouse serum albumin). Free ZSA-51D or diABZI was dissolved in
535 DMSO/PEG-400 (1:4, v/v) and diluted 1:1 with PBS to 0.2 mg/mL for injection; Nano ZSA-51D
536 was directly resuspended in PBS at 0.2 mg/mL. For combination therapy, 100 μg α-PD1 antibodies
537 (Bio X Cell) were given intraperitoneally according to the experimental schedule. For antitumor
538 efficacy, treatments were given every 3 days for 5 doses; for HSPC and immune profiling,
539 treatments were given every 3 days for 3 doses.

540 **In vivo PK study**

541 Free or Nano ZSA-51D (1 mg/kg) was administered intravenously to MC-38 tumor-bearing
542 C57BL/6J mice. Blood and tissues were collected at 15 min, 2 h, and 7 h post-injection. Plasma
543 was separated by centrifugation (15,000 rpm, 10 min). After euthanasia, tumors and hind limb
544 bones were harvested; bone marrow was isolated by brief centrifugation. Samples were stored at
545 −80 °C until analysis. ZSA-51D and ZSA-52D levels were quantified by LC–MS/MS using a
546 Waters XBridge C18 column and a Triple Quad 5500 mass spectrometer (SCIEX) with ESI in
547 positive mode, employing analyte-specific MRM transitions. Results are reported as ng/mL
548 (plasma) or ng/g (tissue).

549 **Single-cell suspension preparation and flow cytometry analysis**

550 Peripheral blood, bone marrow, and tumors were collected after STING agonist treatment. Blood
551 (200 μL) was drawn from ophthalmic veins, and tumors and hind limb bones were harvested post-
552 euthanasia. Bone marrow was flushed with ice-cold PBS + 1% FBS and 1 mM EDTA through a
553 70 μm strainer and centrifuged (350 × g, 5 min). Tumors (<1 g) were minced, digested in RPMI
554 1640 with 0.01–0.1% collagenase/hyaluronidase and 0.15 mg/mL DNase I at 37 °C for 30 min
555 with shaking, filtered, and washed. All suspensions underwent RBC lysis (ACK buffer, 5 min,

556 4 °C), washed, centrifuged (400 × g, 5 min), and resuspended at 1×10^7 cells/mL. Cells were stained
557 with Ghost Dye™ Violet 510 (30 min, 4 °C), blocked with anti-CD16/32 (10 min, 4 °C), then
558 stained with fluorochrome-conjugated antibodies (**Table S1**) for 20 min at 4 °C, washed, fixed
559 (BioLegend), and analyzed on a Cytek Aurora cytometer; data were processed using FlowJo (**Fig.**
560 **S22**).

561 **HSPC analysis**

562 Bone marrow single-cell suspensions were enriched for lineage-negative (Lin^-) cells using a
563 biotin-conjugated lineage panel (BioLegend) and magnetic separation, then stained with
564 fluorophore-conjugated antibodies (**Table S1**) for flow cytometric analysis of HSPC subsets (**Fig.**
565 **S23**).

566 **Cell sorting by FACS**

567 Neutrophils and subpopulations were isolated from bone marrow treated in vitro with vehicle or
568 Nano ZSA-51D (100 nM) using a Sony MA900 sorter with a 100 μm chip at 4 °C. Cells were
569 stained with CD11b, Ly6G, CD101, and CD14, and dead cells excluded with DAPI (5 μg/mL).
570 Neutrophils ($CD11b^+Ly6G^+$) were further gated by CD101 and CD14 to yield $CD101^-CD14^-$,
571 $CD101^-CD14^+$, and $CD101^+CD14^+$ populations. Sorted cells were used for in vitro assays,
572 adoptive transfer, or bulk mRNA analysis. LSK cells ($Lin^-Sca\text{-}1^+c\text{-}Kit^+$) were sorted from enriched
573 bone marrow Lin^- cells.

574 **LSK culture and treatment**

575 Sorted LSK cells were cultured in StemSpan with 50 ng/mL SCF (BioLegend) at 2×10^4 cells/well
576 in 96-well U-bottom plates. Cells were treated with 100 nM Nano ZSA-51D or 10 ng/mL cytokines
577 (TNF-α, IFN-β, IFN-γ, IL-6) for 3 days, then collected, washed, and resuspended in PBS for flow
578 cytometry or bulk mRNA-seq analysis.

579 **In vitro reprogramming of bone marrow neutrophils**

580 Bone marrow cells were isolated from femurs and tibiae of WT or STING KO mice (6–8 weeks).
581 Cells were flushed with PBS + 1% FBS and 1 mM EDTA, centrifuged, RBC-lysed, washed, and
582 resuspended in complete RPMI 1640. Cells (5×10^6/well) were seeded in 12-well plates and treated
583 overnight with 100 nM free or Nano ZSA-51D, vehicle (30 μg/mL mouse serum albumin). In

584 addition, the sorted bone marrow neutrophils were treated with 10 ng ml^{-1} cytokines (TNF-α, IFN-
585 β, IFN-γ, IL-6, TGF-β) for overnight. For TNF-α neutralization, cells were pretreated with TNF-α
586 antibody (10 μg/mL) 2 hours in advance of Nano ZSA-51D treatment. After treatment, cells were
587 collected, washed, and resuspended in PBS for flow cytometry (**Fig. S24**).

588 **Adoptive transfer of neutrophil subsets**

589 Sorted neutrophil subsets ($CD101^{-}CD14^{-}$, $CD101^{-}CD14^{+}$, $CD101^{+}CD14^{+}$; 2×10^{6} cells/mouse)
590 from Nano ZSA-51D–treated bone marrow were adoptively transferred intratumorally into MC-
591 38 tumors, and mice received intraperitoneal α-PD1 (100 μg) every 2 days. Tumor growth and
592 survival were monitored every 2–3 days.

593 **Tumors rechallenge and T cell memory analysis**

594 To assess long-term immunity, cured mice were rechallenged 100–120 days post-treatment with
595 MC-38 or KPC 6642 cells (5×10^{6} cells/mL, 100 μL) subcutaneously, alongside age-matched naïve
596 controls. Tumor growth was monitored every 2–3 days from day 6, and tumor volume was
597 recorded. At 180 days post-rechallenge, spleens, lymph nodes, and blood were collected to prepare
598 single-cell suspensions for flow cytometric analysis of $CD4^{+}$ and $CD8^{+}$ T cell memory (**Fig. S25**).

599 **Bulk mRNA-seq analysis**

600 Total RNA was extracted (RNeasy Plus, QIAGEN), and samples with RIN ⩾ 8 were used. Poly(A)
601 mRNA (250 ng) was isolated (NEBNext Poly(A) Magnetic Isolation), converted to cDNA libraries
602 (NEBNext UltraExpress RNA Library Prep with dual indices), pooled, and sequenced on Illumina
603 NovaSeq X 10B (150 bp paired-end). Adapters and low-quality bases were trimmed with Cutadapt,
604 quality checked with FastQC, and contamination screened with Fastq Screen. Reads were aligned
605 to GRCm38 (ENSEMBL) using STAR, quantified with RSEM, and metrics summarized with
606 MultiQC. Differential expression was analyzed using DESeq2; genes with adjusted $p < 0.05$ and
607 $|\log_2 FC| > 1$ were considered significant. KEGG pathway ORA and GSEA using KEGG/GO gene
608 sets were performed for functional enrichment.

609 **Antigen presentation by neutrophils**

610 Bone marrow cells from WT C57BL/6J mice were seeded at 1×10^{6} cells/well in 24-well plates and
611 treated overnight with OT-I peptide (SIINFEKL, 50 μg/mL), Nano ZSA-51D (100 nM), or vehicle

612 (30 μg/mL mouse serum albumin) in complete RPMI 1640. Cells were collected, washed, and
613 stained with antibodies. MHC I expression and OT-I peptide presentation (H-2Kb/SIINFEKL) on
614 neutrophils and subsets were analyzed by flow cytometry.

615 **OT-I CD8+ T cell activation and proliferation**

616 OT-I $CD8^+$ T cells were isolated (EasySep $CD8^+$ kit, STEMCELL), labeled with CellTrace™
617 Violet, and washed. Bone marrow neutrophils and subsets ($CD101^-CD14^+$, $CD101^+CD14^+$)
618 pretreated with OVA (200 μg/mL), Nano ZSA-51D (100 nM), or vehicle were sorted and co-
619 cultured with labeled T cells at a 2:1 neutrophil:T cell ratio for 48 h; T cells alone served as controls.
620 Cells were imaged by bright-field microscopy (EVOS M5000) and analyzed by flow cytometry
621 for activation markers (CD69, CD25, CD137) and proliferation via CellTrace dilution.

622 **In vivo toxicity assessment**

623 Six-week-old WT C57BL/6J mice (n = 3 per group) received vehicle (15 mg/kg albumin), free, or
624 Nano ZSA-51D (1 mg/kg) intravenously every 3 days for five doses. Blood was collected on days
625 0, 3, and 15 for complete blood counts, and plasma on day 15 for liver function tests. Major organs
626 (heart, liver, spleen, lung, kidney, intestine) were harvested for histopathology. Analyses were
627 performed by the Unit for Laboratory Animal Medicine (ULAM).

628 **Statistical analysis**

629 All statistical analyses were performed using GraphPad Prism (version 10.3.1) unless otherwise
630 specified. Data are presented as mean ± standard deviation (SD). Comparisons between two groups
631 were performed using an unpaired two-tailed Student's T-test. For comparisons involving more
632 than two groups, one-way or two-way analysis of variance (ANOVA) followed by Tukey's or
633 Sidak's multiple comparison test was used as appropriate. For survival analyses, Kaplan–Meier
634 curves were plotted and compared using the log-rank (Mantel–Cox) test. A p-value < 0.05 was
635 considered statistically significant. Specific statistical tests used for each experiment are detailed
636 in the figure legends.

637 **List of Supplementary Materials**

638 Fig. S1 to S25

639 Table S1

Reference:

1 Shaul, M. E. & Fridlender, Z. G. Tumour-associated neutrophils in patients with cancer. *Nat Rev Clin Oncol* **16**, 601-620 (2019). https://doi.org:10.1038/s41571-019-0222-4

2 Veglia, F., Sanseviero, E. & Gabrilovich, D. I. Myeloid-derived suppressor cells in the era of increasing myeloid cell diversity. *Nat Rev Immunol* **21**, 485-498 (2021). https://doi.org:10.1038/s41577-020-00490-y

3 Hedrick, C. C. & Malanchi, I. Neutrophils in cancer: heterogeneous and multifaceted. *Nat Rev Immunol* **22**, 173-187 (2022). https://doi.org:10.1038/s41577-021-00571-6

4 Jaillon, S. *et al.* Neutrophil diversity and plasticity in tumour progression and therapy. *Nat Rev Cancer* **20**, 485-503 (2020). https://doi.org:10.1038/s41568-020-0281-y

5 Huang, X. *et al.* Neutrophils in Cancer immunotherapy: friends or foes? *Mol Cancer* **23**, 107 (2024). https://doi.org:10.1186/s12943-024-02004-z

6 Zhang, M., Qin, H., Wu, Y. & Gao, Q. Complex role of neutrophils in the tumor microenvironment: an avenue for novel immunotherapies. *Cancer Biol Med* **21**, 849-863 (2024). https://doi.org:10.20892/j.issn.2095-3941.2024.0192

7 Eruslanov, E., Nefedova, Y. & Gabrilovich, D. I. The heterogeneity of neutrophils in cancer and its implication for therapeutic targeting. *Nat Immunol* **26**, 17-28 (2025). https://doi.org:10.1038/s41590-024-02029-y

8 Su, J. L. *et al.* Pretreatment neutrophil-to-lymphocyte ratio is associated with immunotherapy efficacy in patients with advanced cancer: a systematic review and meta-analysis. *Sci Rep-Uk* **15** (2025). https://doi.org:ARTN 44610.1038/s41598-024-84890-3

9 Mitchell, K. G. *et al.* Neutrophil expansion defines an immunoinhibitory peripheral and intratumoral inflammatory milieu in resected non-small cell lung cancer: a descriptive analysis of a prospectively immunoprofiled cohort. *J Immunother Cancer* **8** (2020). https://doi.org:ARTN e00040510.1136/jitc-2019-000405

10 Gungabeesoon, J. *et al.* A neutrophil response linked to tumor control in immunotherapy. *Cell* **186**, 1448-1464 e1420 (2023). https://doi.org:10.1016/j.cell.2023.02.032

11 Linde, I. L. *et al.* Neutrophil-activating therapy for the treatment of cancer. *Cancer Cell* **41**, 356-+ (2023). https://doi.org:10.1016/j.ccell.2023.01.002

12 Li, M., Ng, M. & Ng, L. G. Firing up neutrophil anti-tumor immunity with cocktails. *Cancer Cell* **41**, 227-229 (2023). https://doi.org:10.1016/j.ccell.2023.01.005

13 Hirschhorn, D. *et al.* T cell immunotherapies engage neutrophils to eliminate tumor antigen escape variants. *Cell* **186**, 1432-+ (2023). https://doi.org:10.1016/j.cell.2023.03.007

14 Kumbhojkar, N. *et al.* Neutrophils bearing adhesive polymer micropatches as a drug-free cancer immunotherapy. *Nat Biomed Eng* **8** (2024). https://doi.org:10.1038/s41551-024-01180-z

15 Ager, A. Cancer immunotherapy: T cells and neutrophils working together to attack cancers. *Cell* **186**, 1304-1306 (2023). https://doi.org:10.1016/j.cell.2023.03.005

16 Benguigui, M. *et al*. Interferon-stimulated neutrophils as a predictor of immunotherapy response. *Cancer Cell* **42** (2024). https://doi.org:10.1016/j.ccell.2023.12.005

17 Wu, Y. *et al*. Neutrophil profiling illuminates anti-tumor antigen-presenting potency. *Cell* **187**, 1422-1439 e1424 (2024). https://doi.org:10.1016/j.cell.2024.02.005

18 Mysore, V. *et al*. FcγR engagement reprograms neutrophils into antigen cross-presenting cells that elicit acquired anti-tumor immunity. *Nature Communications* **12** (2021). https://doi.org:ARTN 479110.1038/s41467-021-24591-x

19 Ozel, I. *et al*. Neutrophil-specific targeting of STAT3 impairs tumor progression via the expansion of cytotoxic CD8(+) T cells. *Signal Transduct Target Ther* **10**, 279 (2025). https://doi.org:10.1038/s41392-025-02363-z

20 Garner, H. *et al*. Understanding and reversing mammary tumor-driven reprogramming of myelopoiesis to reduce metastatic spread. *Cancer Cell* (2025). https://doi.org:10.1016/j.ccell.2025.04.007

21 Dong, L. & Ng, L. G. Tumor neutrophils rewired from birth. *Cancer Cell* (2025). https://doi.org:10.1016/j.ccell.2025.05.005

22 Giles, A. J. *et al*. Activation of Hematopoietic Stem/Progenitor Cells Promotes Immunosuppression Within the Pre-metastatic Niche. *Cancer Research* **76**, 1335-1347 (2016). https://doi.org:10.1158/0008-5472.Can-15-0204

23 Daman, A. W. *et al*. Microbial cancer immunotherapy reprograms hematopoiesis to enhance myeloid-driven anti-tumor immunity. *Cancer Cell* (2025). https://doi.org:10.1016/j.ccell.2025.05.002

24 Qian, J. *et al*. A CXCR4 partial agonist improves immunotherapy by targeting immunosuppressive neutrophils and cancer-driven granulopoiesis. *Cancer Cell* **43**, 1512-1529 e1511 (2025). https://doi.org:10.1016/j.ccell.2025.06.006

25 Hegde, S. *et al*. Myeloid progenitor dysregulation fuels immunosuppressive macrophages in tumours. *Nature* (2025). https://doi.org:10.1038/s41586-025-09493-y

26 Alicea-Torres, K. *et al*. Immune suppressive activity of myeloid-derived suppressor cells in cancer requires inactivation of the type I interferon pathway. *Nat Commun* **12**, 1717 (2021). https://doi.org:10.1038/s41467-021-22033-2

27 Sun, Y. Y. *et al*. The downregulation of type I IFN signaling in G-MDSCs under tumor conditions promotes their development towards an immunosuppressive phenotype. *Cell Death Dis* **13** (2022). https://doi.org:ARTN 3610.1038/s41419-021-04487-w

28 Ishikawa, H. & Barber, G. N. STING is an endoplasmic reticulum adaptor that facilitates innate immune signalling. *Nature* **455**, 674-U674 (2008). https://doi.org:10.1038/nature07317

29 Ishikawa, H., Ma, Z. & Barber, G. N. STING regulates intracellular DNA-mediated, type I interferon-dependent innate immunity. *Nature* **461**, 788-U740 (2009). https://doi.org:10.1038/nature08476

30 Balka, K. R. *et al*. TBK1 and IKKε Act Redundantly to Mediate STING-Induced NF-κB Responses in Myeloid Cells. *Cell Rep* **31** (2020). https://doi.org:ARTN 10749210.1016/j.celrep.2020.03.056

31 Liao, W. N., Du, C. H. & Wang, J. P. The cGAS-STING Pathway in Hematopoiesis and Its Physiopathological Significance. *Front Immunol* **11** (2020). https://doi.org:ARTN 57391510.3389/fimmu.2020.573915

32 Xie, J. Y. *et al*. STING activation in TET2-mutated hematopoietic stem/progenitor cells contributes to the increased self-renewal and neoplastic transformation. *Leukemia* **37**, 2457-2467 (2023). https://doi.org:10.1038/s41375-023-02055-z

33 Zhao, H. Y. *et al*. An oral tricyclic STING agonist suppresses tumor growth through remodeling of the immune microenvironment. *Cell Chem Biol* **32** (2025). https://doi.org:10.1016/j.chembiol.2025.01.004

34 Hoogenboezem, E. N. & Duvall, C. L. Harnessing albumin as a carrier for cancer therapies. *Adv Drug Deliver Rev* **130**, 73-89 (2018). https://doi.org:10.1016/j.addr.2018.07.011

35 Song, Y. D. *et al*. Albumin nanoparticle containing a PI3Kγ inhibitor and paclitaxel in combination with α-PD1 induces tumor remission of breast cancer in mice. *Sci Transl Med* **14** (2022). https://doi.org:ARTN eabl364910.1126/scitranslmed.abl3649

36 Sun, D., Zhou, S. & Gao, W. What Went Wrong with Anticancer Nanomedicine Design and How to Make It Right. *ACS Nano* **14**, 12281-12290 (2020). https://doi.org:10.1021/acsnano.9b09713

37 Pietras, E. M. *et al*. Functionally Distinct Subsets of Lineage-Biased Multipotent Progenitors Control Blood Production in Normal and Regenerative Conditions. *Cell Stem Cell* **17**, 35-46 (2015). https://doi.org:10.1016/j.stem.2015.05.003

38 Singhal, S. *et al*. Origin and Role of a Subset of Tumor-Associated Neutrophils with Antigen-Presenting Cell Features in Early-Stage Human Lung Cancer. *Cancer Cell* **30**, 120-135 (2016). https://doi.org:10.1016/j.ccell.2016.06.001

39 Saha, S. & Biswas, S. K. Tumor-Associated Neutrophils Show Phenotypic and Functional Divergence in Human Lung Cancer. *Cancer Cell* **30**, 11-13 (2016). https://doi.org:10.1016/j.ccell.2016.06.016

40 Liu, C. Y. *et al*. Population alterations of L-arginase- and inducible nitric oxide synthase-expressed CD11b+/CD14(-)/CD15+/CD33+ myeloid-derived suppressor cells and CD8+ T lymphocytes in patients with advanced-stage non-small cell lung cancer. *J Cancer Res Clin Oncol* **136**, 35-45 (2010). https://doi.org:10.1007/s00432-009-0634-0

41 Evrard, M. *et al*. Developmental Analysis of Bone Marrow Neutrophils Reveals Populations Specialized in Expansion, Trafficking, and Effector Functions. *Immunity* **48**, 364-379 e368 (2018). https://doi.org:10.1016/j.immuni.2018.02.002

42 Muendlein, H. I. *et al*. Neutrophils and macrophages drive TNF-induced lethality via TRIF/CD14-mediated responses. *Science Immunology* **7** (2022). https://doi.org:ARTN eadd066510.1126/sciimmunol.add0665

43 Hackert, N. S. *et al*. Human and mouse neutrophils share core transcriptional programs in both homeostatic and inflamed contexts. *Nature Communications* **14** (2023). https://doi.org:ARTN 813310.1038/s41467-023-43573-9

765 44 Sharygin, D., Koniaris, L. G., Wells, C., Zimmers, T. A. & Hamidi, T. Role of CD14 in
766 human disease. *Immunology* **169**, 260-270 (2023).
767 https://doi.org:10.1111/imm.13634
768 45 Pugin, J. *et al.* Cd14 Is a Pattern-Recognition Receptor. *Immunity* **1**, 509-516 (1994).
769 https://doi.org:Doi 10.1016/1074-7613(94)90093-0
770 46 Ding, Z. M. *et al.* Relative contribution of LFA-1 and Mac-1 to neutrophil adhesion and
771 migration. *J Immunol* **163**, 5029-5038 (1999).
772 47 Carlos, T. M. & Harlan, J. M. Leukocyte-Endothelial Adhesion Molecules. *Blood* **84**,
773 2068-2101 (1994).
774 48 Fridlender, Z. G. *et al.* Polarization of Tumor-Associated Neutrophil Phenotype by TGF-
775 β: "N1" versus "N2" TAN. *Cancer Cell* **16**, 183-194 (2009).
776 https://doi.org:10.1016/j.ccr.2009.06.017
777 49 Piccard, H., Muschel, R. J. & Opdenakker, G. On the dual roles and polarized
778 phenotypes of neutrophils in tumor development and progression. *Crit Rev Oncol*
779 *Hematol* **82**, 296-309 (2012). https://doi.org:10.1016/j.critrevonc.2011.06.004
780 50 Zhang, J. *et al.* Engineering and Targeting Neutrophils for Cancer Therapy. *Adv Mater*
781 **36**, e2310318 (2024). https://doi.org:10.1002/adma.202310318
782 51 Kawai, T. & Akira, S. Toll-like Receptors and Their Crosstalk with Other Innate
783 Receptors in Infection and Immunity. *Immunity* **34**, 637-650 (2011).
784 https://doi.org:10.1016/j.immuni.2011.05.006
785 52 Kawai, T. & Akira, S. The roles of TLRs, RLRs and NLRs in pathogen recognition. *Int*
786 *Immunol* **21**, 317-337 (2009). https://doi.org:10.1093/intimm/dxp017
787 53 Wicherska-Pawlowska, K., Wrobel, T. & Rybka, J. Toll-Like Receptors (TLRs), NOD-Like
788 Receptors (NLRs), and RIG-I-Like Receptors (RLRs) in Innate Immunity. TLRs, NLRs,
789 and RLRs Ligands as Immunotherapeutic Agents for Hematopoietic Diseases. *Int J*
790 *Mol Sci* **22** (2021). https://doi.org:ARTN 1339710.3390/ijms222413397

791 54 Yan, H. M., Kamiya, T., Suabjakyong, P. & Tsuji, N. M. Targeting C-type lectin receptors
792 for cancer immunity. *Front Immunol* **6** (2015). https://doi.org:ARTN
793 40810.3389/fimmu.2015.00408

794 55 Li, J. Y. *et al.* Tumor Cell-Intrinsic Factors Underlie Heterogeneity of Immune Cell
795 Infiltration and Response to Immunotherapy. *Immunity* **49**, 178-+ (2018).
796 https://doi.org:10.1016/j.immuni.2018.06.006
797 56 Reynaud, D. *et al.* IL-6 Controls Leukemic Multipotent Progenitor Cell Fate and
798 Contributes to Chronic Myelogenous Leukemia Development. *Cancer Cell* **20**, 661-
799 673 (2011). https://doi.org:10.1016/j.ccr.2011.10.012
800 57 Zhao, J. L. *et al.* Conversion of Danger Signals into Cytokine Signals by Hematopoietic
801 Stem and Progenitor Cells for Regulation of Stress-Induced Hematopoiesis. *Cell*
802 *Stem Cell* **14**, 445-459 (2014). https://doi.org:10.1016/j.stem.2014.01.007
803 58 Tie, R. X. *et al.* Interleukin-6 signaling regulates hematopoietic stem cell emergence.
804 *Exp Mol Med* **51** (2019). https://doi.org:ARTN 12410.1038/s12276-019-0320-5

59 Kimmel, B. R. *et al*. Potentiating cancer immunotherapies with modular albumin-hitchhiking nanobody-STING agonist conjugates. *Nat Biomed Eng* (2025). https://doi.org:10.1038/s41551-025-01400-0

60 Nagata, M. *et al*. A critical role of STING-triggered tumor-migrating neutrophils for anti-tumor effect of intratumoral cGAMP treatment. *Cancer Immunol Immun* **70**, 2301-2312 (2021). https://doi.org:10.1007/s00262-021-02864-0

61 Xu, T. X. *et al*. Systemic administration of STING agonist promotes myeloid cells maturation and antitumor immunity through regulating hematopoietic stem and progenitor cell fate. *Cancer Immunol Immun* (2023). https://doi.org:10.1007/s00262-023-03502-7

62 Zanoni, I., Tan, Y. H., Di Gioia, M., Springstead, J. R. & Kagan, J. C. By Capturing Inflammatory Lipids Released from Dying Cells, the Receptor CD14 Induces Inflammasome-Dependent Phagocyte Hyperactivation. *Immunity* **47**, 697-+ (2017). https://doi.org:10.1016/j.immuni.2017.09.010

63 Schröder, N. W. J. *et al*. Lipoteichoic acid (LTA) of and activates immune cells via toll-like receptor (TLR)-2, lipopolysaccharide-binding protein (LBP), and CD14, whereas TLR-4 and MD-2 are not involved. *J Biol Chem* **278**, 15587-15594 (2003). https://doi.org:10.1074/jbc.M212829200

64 Roedig, H. *et al*. Biglycan is a new high-affinity ligand for CD14 in macrophages. *Matrix Biol* **77**, 4-22 (2019). https://doi.org:10.1016/j.matbio.2018.05.006

65 Woodfin, A. *et al*. ICAM-1-expressing neutrophils exhibit enhanced effector functions in murine models of endotoxemia. *Blood* **127**, 898-907 (2016). https://doi.org:10.1182/blood-2015-08-664995

66 Lee, S. H. *et al*. Intracellular Adhesion Molecule-1 Improves Responsiveness to Immune Checkpoint Inhibitor by Activating CD8 T Cells. *Adv Sci* **10** (2023). https://doi.org:10.1002/advs.202204378

67 Ma, V. P. Y. *et al*. The magnitude of LFA-1/ICAM-1 forces fine-tune TCR-triggered T cell activation. *Sci Adv* **8** (2022). https://doi.org:ARTN eabg448510.1126/sciadv.abg4485

68 Deeths, M. J. & Mescher, M. F. ICAM-1 and B7-1 provide similar but distinct costimulation for CD8+ T cells, while CD4+ T cells are poorly costimulated by ICAM-1. *Eur J Immunol* **29**, 45-53 (1999).

69 Cox, M. A., Barnum, S. R., Bullard, D. C. & Zajac, A. J. ICAM-1-dependent tuning of memory CD8 T-cell responses following acute infection. *P Natl Acad Sci USA* **110**, 1416-1421 (2013). https://doi.org:10.1073/pnas.1213480110

70 Eruslanov, E. B. *et al*. Tumor-associated neutrophils stimulate T cell responses in early-stage human lung cancer. *Journal of Clinical Investigation* **124**, 5466-5480 (2014). https://doi.org:10.1172/Jci77053

71 Hines, J. B., Kacew, A. J. & Sweis, R. F. The Development of STING Agonists and Emerging Results as a Cancer Immunotherapy. *Curr Oncol Rep* **25**, 189-199 (2023). https://doi.org:10.1007/s11912-023-01361-0

72 Motedayen Aval, L., Pease, J. E., Sharma, R. & Pinato, D. J. Challenges and Opportunities in the Clinical Development of STING Agonists for Cancer Immunotherapy. *J Clin Med* **9** (2020). https://doi.org:10.3390/jcm9103323

73 Wang, B. *et al.* Clinical applications of STING agonists in cancer immunotherapy: current progress and future prospects. *Front Immunol* **15**, 1485546 (2024). https://doi.org:10.3389/fimmu.2024.1485546

74 Ramanjulu, J. M. *et al.* Design of amidobenzimidazole STING receptor agonists with systemic activity. *Nature* **564**, 439-443 (2018). https://doi.org:10.1038/s41586-018-0705-y

75 Chin, E. N. *et al.* Antitumor activity of a systemic STING-activating non-nucleotide cGAMP mimetic. *Science* **369**, 993-999 (2020). https://doi.org:10.1126/science.abb4255

76 Pan, B. S. *et al.* An orally available non-nucleotide STING agonist with antitumor activity. *Science* **369**, 935-+ (2020). https://doi.org:ARTN aba609810.1126/science.aba6098

77 Zhao, H. Y. *et al.* Design of an Oral STING Agonist through Intramolecular Hydrogen Bond Ring Mimicking to Achieve Complete Tumor Regression. *J Med Chem* **68**, 11365-11385 (2025). https://doi.org:10.1021/acs.jmedchem.5c00296

Acknowledgements

We thank the University of Michigan Unit for Laboratory Animal Medicine (ULAM) for support in maintaining laboratory animals, and the In Vivo Animal Core (IVAC) for assistance toxicity studies. We also acknowledge the University of Michigan Pharmacokinetics Core, Flow Cytometry Core, Genomics Core for technical service.

Author contributions

J.T., W.G., and D.S. conceived the project, developed the hypotheses, designed the experiments and wrote the manuscript; J.T. performed most experiments and analyzed data, with assistance from all authors; H.Z. conducted the chemical synthesis. C.L. provided support for bioinformatic analysis. H.W. and F.K. assisted with the in vivo flow cytometry studies. Q.L., M.H. and B.W. assisted with the in vivo pharmacokinetic studies. Z.L. tested the STING binding and cellular activity in vitro. D.S. supervised the project and acquired funding.

Competing interests

University of Michigan has filed a patent based on these studies where some authors are listed as inventors.

Data and materials availability

All data associated with this study are present in the paper or the Supplementary Materials. Materials can be made available through a material transfer agreement with D.S.

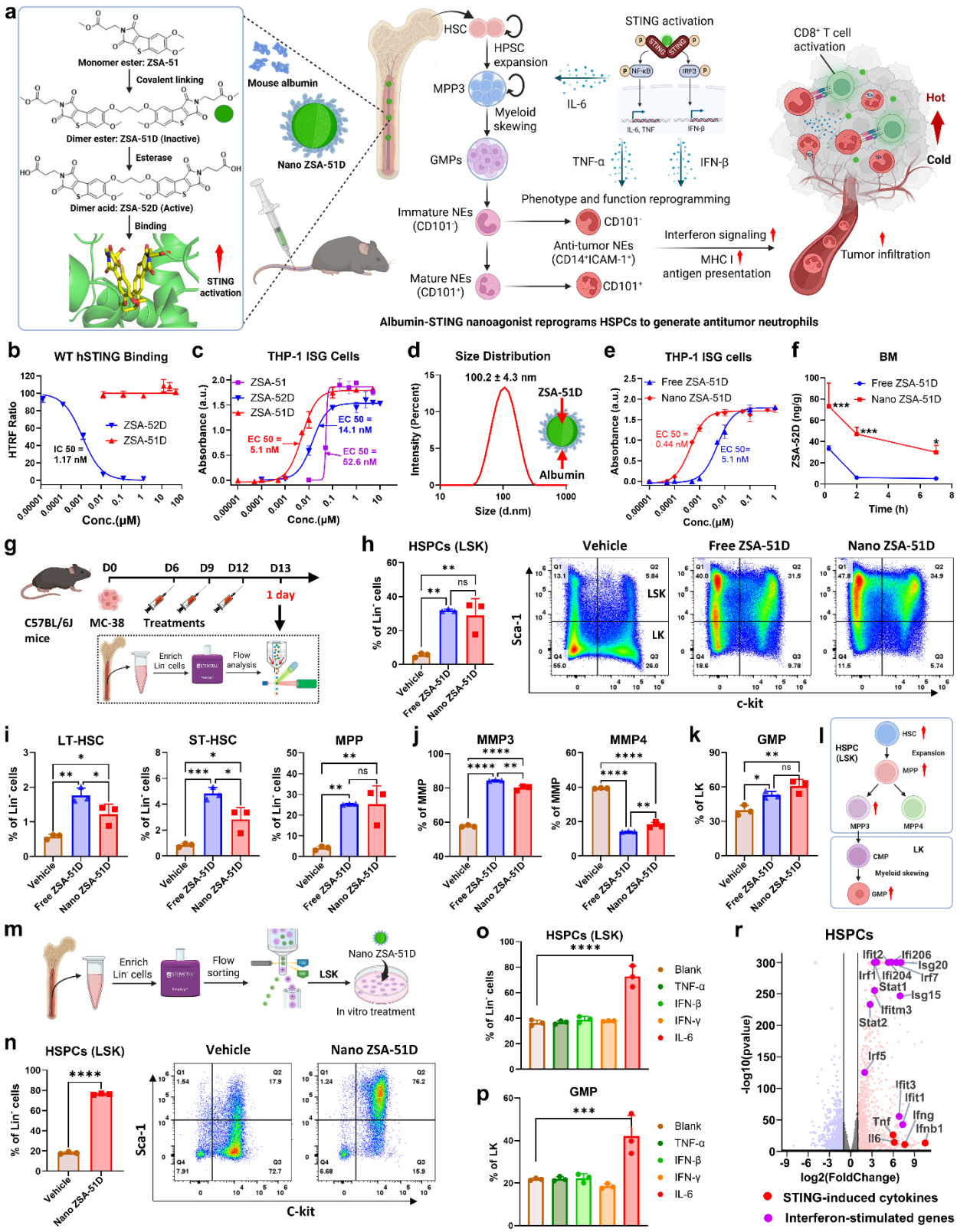

Figure 1. Nano ZSA-51D potently activates STING pathway to expand HSPCs and promote GMP differentiation with strong interferon signaling.

(a) Schematic illustration of Nano ZSA-51D that reprograms HSPCs into antitumor neutrophils for cancer immunotherapy. Dimeric STING agonist ZSA-51D derived from monomeric STING agonist ZSA-51 was encapsulated into mouse albumin to form Nano ZSA-51D. Chemical structures of ZSA-51, ZSA-51D and its acid form, ZSA-52D, along with molecular docking simulation showing ZSA-52D (yellow) binding to the STING protein (green, PDB: 6UKZ), performed using AutoDock. Nano ZSA-51D expands HSPCs and skews GMP differentiation via STING–NF-κB–IL-6 signaling, which further reprograms immature ($CD101^{-}$) and mature ($CD101^{+}$) bone marrow neutrophils into $CD14^{+}ICAM\text{-}1^{+}$ subsets through STING–NF-κB–TNF-α signaling, upregulating interferon signaling and MHC I antigen presentation to promote $CD8^{+}$ T cell antitumor responses.

(b) Binding affinity of ZSA-51D and ZSA-52D to wild-type (WT) human STING (hSTING) protein, determined by Homogeneous Time-Resolved Fluorescence (HTRF) assay (n=3).

(c) STING pathway activation was assessed in THP1-Blue ISG reporter cells with virous concentrations of ZSA-51D and ZSA-52D for 24 hours, demonstrating induction of the STING–IRF signaling cascade (n=3).

(d) Particle size distribution and schematic structure of Nano ZSA-51D.

(e) Comparison of STING-IRF pathway activation by free and Nano ZSA-51D in THP1-Blue ISG reporter cells after 24-hour treatment (n=3).

(f) Pharmacokinetic profiles of Free and Nano ZSA-51D (1 mg/kg, I.V.), showing concentrations of ZSA-52D (acid form) in bone marrow at 15 minutes, 2 hours and 7 hours post-injection, quantified via LC-MS/MS (n = 3). * $p < 0.05$, *** $p < 0.001$ vs. Free ZSA-51D.

(g) Schematic illustration of treatment schedule and flow cytometry analysis to examine the composition of HSPC subsets in bone marrow of MC-38 tumor bearing mice 24 hours post-treatment. The flow cytometry analysis of HSPCs was performed after enrichment of Lin^{-} cells.

(h) Quantification (left) and representative flow cytometry plots (right) of HSPCs ($Lin^{-}Sca\text{-}1^{+}c\text{-}Kit^{+}$, LSK) within Lin^{-} cells in bone marrow following free or Nano ZSA-51D treatment (n = 3). **$p < 0.01$, ns: not significant.

(i) Quantification (left) of LT-HSC ($CD150^{+}CD48^{-}$), ST-HSC ($CD150^{-}CD48^{-}$) and MPP ($CD150^{-/+}CD48^{+}$) within Lin^{-} cells in bone marrow following free or Nano ZSA-51D treatment (n = 3). *$p < 0.05$, **$p < 0.01$, ***$p < 0.001$, ns: not significant.

(j) Quantification of myeloid-biased multipotent progenitor 3 (MPP3, $CD34^{+}CD135^{-}$) and lymphoid-biased multipotent progenitor 4 (MPP4, $CD34^{+}CD135^{+}$) within MMP ($Lin^{-}Sca\text{-}1^{+}c\text{-}Kit^{+}CD150^{-/+}CD48^{+}$) in bone marrow following free or Nano ZSA-51D treatment (n = 3). ****$p < 0.0001$, ns: not significant.

(k) Quantification of granulocyte-monocyte progenitor (GMP, $CD150^{-}CD16/32^{+}$) within LK ($Lin^{-}Sca\text{-}1^{-}c\text{-}Kit^{+}$) in bone marrow following free or Nano ZSA-51D treatment (n = 3). *$p < 0.05$, **$p < 0.01$, ns: not significant.

(l) Schematic illustration of HSPCs expansion and skewing differentiation toward GMP after STING agonist treatments. HSC, hematopoietic stem cell; MPP, multipotent progenitor; MPP3, myeloid-biased multipotent progenitor 3; MPP4, lymphoid-biased multipotent progenitor 4; CMP, common myeloid progenitor; GMP (granulocyte-monocyte progenitor).

926 **(m)** Experimental schematic of the in vitro treatment of LSK via Nano ZSA-51D (100 nM). The
927 LSK ($Lin^{-}Sca\text{-}1^{+}c\text{-}Kit^{+}$) was sorted by flow after enrichment of Lin- cells from bone marrow cells.
928 **(n)** Quantification (left) and representative flow cytometry plots (right) of LSK ($Lin^{-}Sca\text{-}1^{+}c\text{-}Kit^{+}$)
929 within Lin^{-} cells following in vitro treatment of Nano ZSA-51D for 3 days (n = 3). ****$p < 0.0001$.
930 **(o, p)** Quantification (left) and representative flow cytometry plots (right) of HSPCs ($Lin^{-}Sca\text{-}1^{+}c\text{-}$
931 Kit^{+}, LSK) within Lin^{-} cells (i) and GMP ($CD150^{-}CD16/32^{+}$) within LK ($Lin^{-}Sca\text{-}1^{-}c\text{-}Kit^{+}$) (j)
932 following in vitro treatments of the STING pathway downstream cytokines (TNF-α, IFN-β, IFN-
933 γ and IL-6) for 3 days (n = 3). ***$p < 0.001$, ****$p < 0.0001$.
934 **(r)** Volcano plot of differentially expressed gene analysis between vehicle and Nano ZSA-51D
935 treated HSPCs. Significance threshold for P adjusted value was 0.01 and foldchange was 2. The
936 STING-induced cytokines (red dots) and interferon-stimulated genes (purple dots) were
937 highlighted.

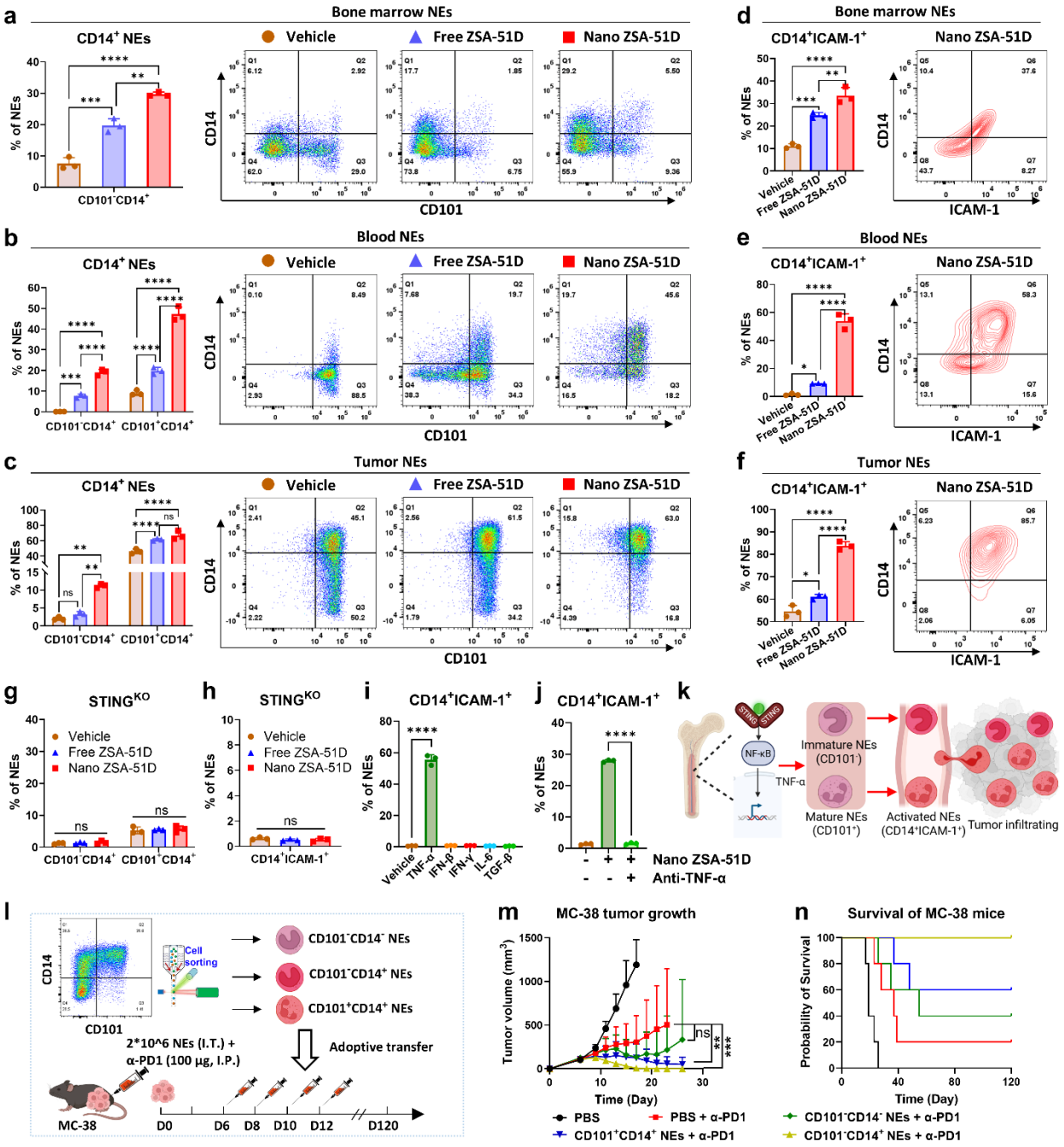

Figure 2. Nano ZSA-51D reprograms bone marrow neutrophils into CD14$^+$ICAM-1$^+$ antitumor subset via STING–NF-κB–TNF-α signaling, driving complete MC-38 tumor remission with α-PD1 therapy.

(a-c) Quantification (left) and representative flow cytometry plots (right) of CD101$^-$CD14$^+$ and CD101$^+$CD14$^+$ neutrophil (NE) subtypes in bone marrow (a), blood (b) and tumors (c) of MC-38 tumor-bearing C57BL/6J mice 24 hours after systemic administration of free and Nano ZSA-51D (1 mg/kg) (n = 3). **p < 0.01, ***p < 0.001, ****p < 0.0001, ns: not significant.

(d-f) Quantification (left) and representative flow cytometry plots (right) of $CD14^+ICAM\text{-}1^+$ neutrophil subtypes in bone marrow (d), blood (e) and tumors (f) after systemic administration of Nano ZSA-51D (1 mg/kg) (n = 3). *p < 0.05, **p < 0.01, ***p < 0.001, ****p < 0.0001.

(g-h) Quantification of $CD101^-CD14^+$, $CD101^+CD14^+$ (g) and $CD14^+ICAM\text{-}1^+$ (h) neutrophils after overnight in vitro treatments with free and Nano ZSA-51D (100 nM) in bone marrow cells from STING knockout mice (C57BL/6J-Sting1gt/J) (n = 3). ns: not significant.

(i) Quantification of $CD14^+ICAM\text{-}1^+$ neutrophils following in vitro treatments of the STING pathway downstream cytokines (TNF-α, IFN-β, IFN-γ and IL-6) for overnight. The immunosuppressive TGF-β as control (n = 3). ****p < 0.0001.

(j) Quantification and changes of $CD14^+ICAM\text{-}1^+$ neutrophils after overnight in vitro treatment with Nano ZSA-51D (100 nM) and TNF-α neutralization (10 μg/ml anti-TNF-α) (n=3). ****p < 0.0001.

(k) Schematic illustration of STING activation-induced reprogramming of immature ($CD101^-$) and mature ($CD101^+$) bone marrow neutrophils into activated $CD14^+ICAM\text{-}1^+$ subsets with enhanced tumor infiltration.

(l) Schematic experiment of neutrophil adoptive transfer. $CD101^-CD14^-$, $CD101^-CD14^+$ and $CD101^+CD14^+$ neutrophils (NEs) were sorted from bone marrow cells pretreated overnight with Nano ZSA-51D (100 nM), then intratumorally injected into MC-38 tumor-bearing mice alongside intraperitoneal α-PD1 (100 μg/mouse).

(**m, n**) Tumor growth curves (l) and survival curves (m) of MC-38 tumor-bearing mice after adoptive transfer of $CD101^-CD14^-$, $CD101^-CD14^+$ or $CD101^+CD14^+$ neutrophils in combination with α-PD1 (100 μg/mice) treatments (n=5). **p < 0.01, ***p < 0.001, ns: not significant. Survival comparisons were performed using a log-rank (Mantel–Cox) test.

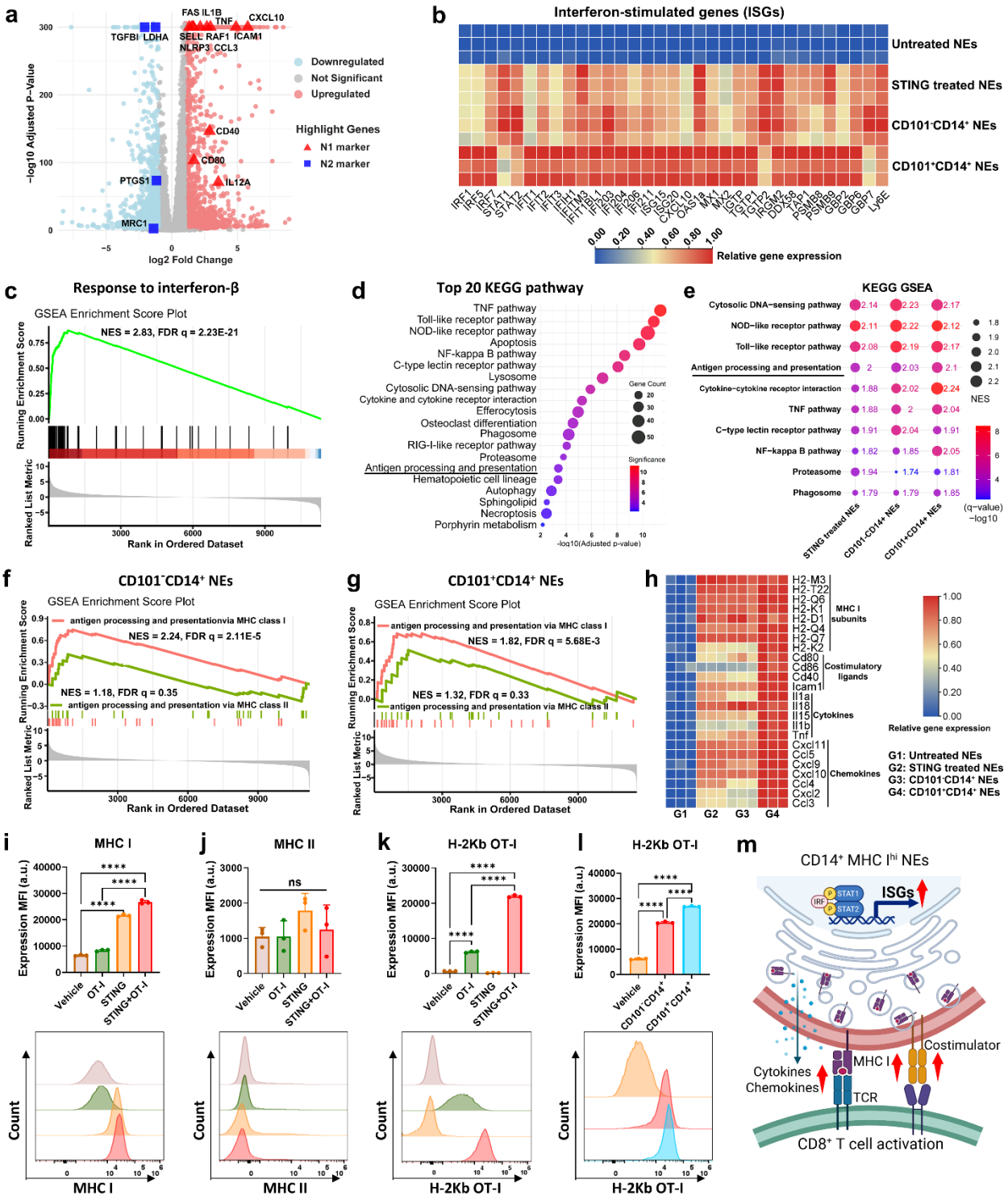

Figure 3. Nano ZSA-51D enhances interferon signaling and MHC I antigen presentation in neutrophils.

(a) Volcano plot of differentially expressed gene analysis between vehicle and Nano ZSA-51D treated neutrophils. Significance threshold for P adjusted value was 0.01 and foldchange was 2.

975 The antitumor (N1, red triangle) and protumor (N2, blue square) neutrophil markers were
976 highlighted.
977 **(b)** Heatmap of relative interferon-stimulated gene (ISG) expression in Nano ZSA-51D-treated
978 neutrophils (NEs) and their $CD101^{-}CD14^{+}$ and $CD101^{+}CD14^{+}$ subtypes, compared to untreated
979 neutrophils.
980 **(c)** Gene Ontology (GO) GESA enrichment score plots for biological process that response to
981 interferon-beta (IFN-β) in Nano ZSA-51D treated neutrophils.
982 **(d)** Top 20 KEGG pathway enrichment analysis based on the differentially expressed genes (DEGs)
983 in neutrophils from Nano ZSA-51D-treated and vehicle-treated groups, ranked by adjusted p-
984 values.
985 **(e)** Top 10 upregulated pathways in Nano ZSA-51D-treated neutrophils and their $CD101^{-}CD14^{+}$
986 and $CD101^{+}CD14^{+}$ subtypes, identified by KEGG Gene Set Enrichment Analysis (GESA).
987 Normalized enrichment score (NES > 1.5) indicates significant upregulation. FDR q-value ($q <$
988 0.05) denotes statistical significance after false discovery rate adjustment.
989 (**f, g**) Gene Ontology (GO) GESA enrichment score plots for antigen processing and presentation
990 via MHC class I and II in $CD101^{-}CD14^{+}$ (f) and $CD101^{+}CD14^{+}$ (g) neutrophils. Normalized
991 enrichment score (NES > 1.5) indicates significant upregulation. FDR q-value ($q < 0.05$) denotes
992 statistical significance after false discovery rate adjustment.
993 **(h)** Heatmap of relative gene expression of MHC class I subunits, costimulatory ligands, T cell-
994 activating cytokines and T cell-recruiting chemokines in Nano ZSA-51D-treated neutrophils and
995 their $CD101^{-}CD14^{+}$ and $CD101^{+}CD14^{+}$ subtypes.
996 (**i, j**) Protein expression of MHC class I (i) and II (j) molecules on bone marrow neutrophils
997 following treatments with OT-I or/and Nano ZSA-51D (n = 3). ****$p < 0.0001$, ns: not significant.
998 (**k**) Presentation of OT-I peptide via MHC class I ($H\text{-}2K^{b}$-OT-I complex) on neutrophils following
999 treatments with OT-I or/and Nano ZSA-51D (n = 3). ****$p < 0.0001$.
1000 (**l**) Presentation of OT-I peptide via MHC class I ($H\text{-}2K^{b}$-OT-I complex) on $CD101^{-}CD14^{+}$ and
1001 $CD101^{+}CD14^{+}$ neutrophils following OT-I treatment (n = 3). ****$p < 0.0001$.
1002 **(m)** Schematic illustration of antigen presentation by ISG-expressing $CD14^{+}$MHC I^{hi} neutrophils
1003 via MHC class I to activate $CD8^{+}$ T cells.

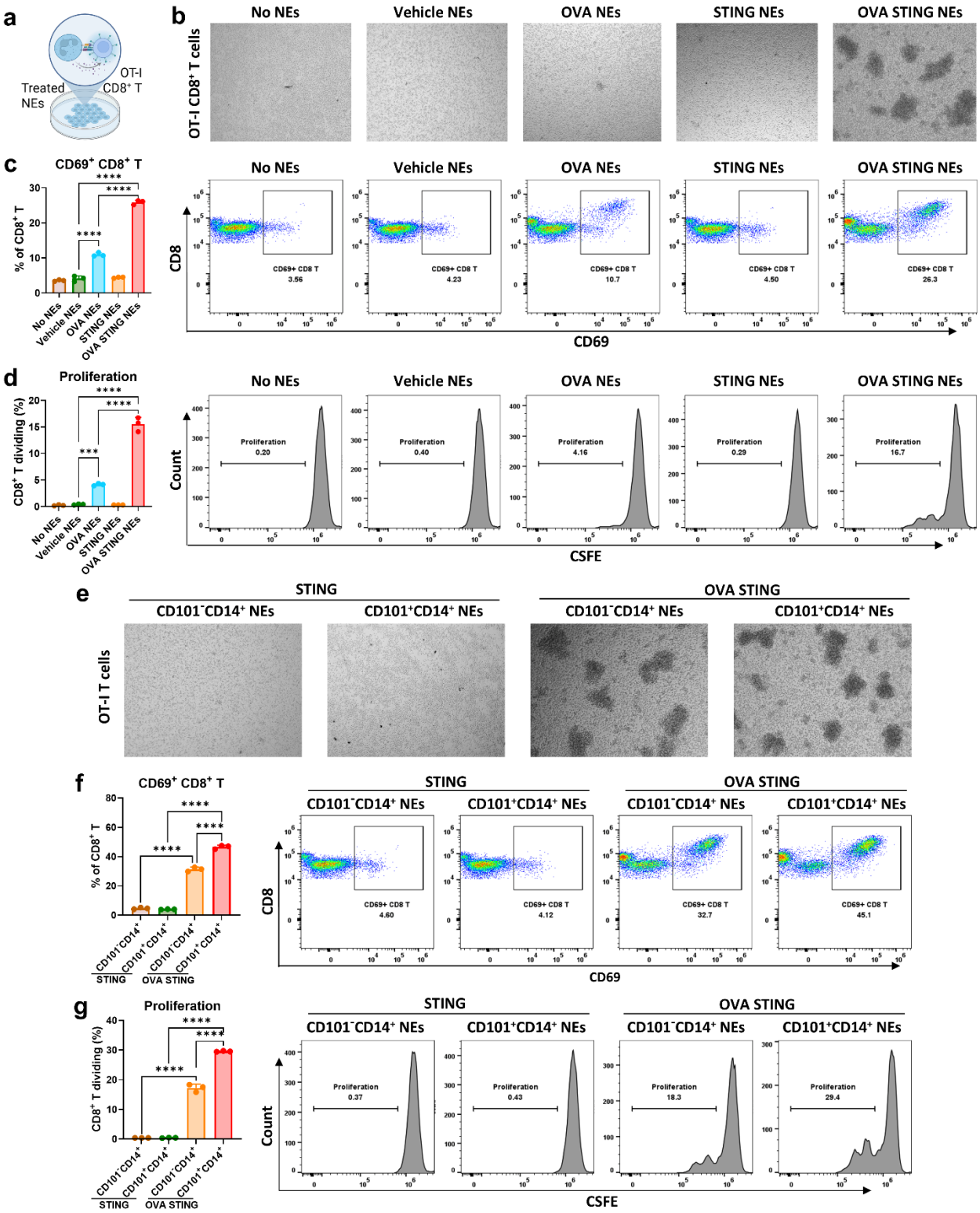

Figure 4. Nano ZSA-51D-reprogrammed neutrophils prime antigen-specific CD8$^+$ T cell responses.

1007 **(a)** Experimental schematic showing Nano ZSA-51D (100 Nm) and OVA (0.2 mg/ml) pre-treated
1008 neutrophils (NEs) co-incubated with OT-I $CD8^+$ T cells for 48 hours.
1009 **(b)** Bright-field microscopy images of OT-I $CD8^+$ T cells after co-incubation with differently
1010 treated bone marrow neutrophils (NEs) for 48 hours. Neutrophils were sorted from bone marrow
1011 pretreated overnight with OVA (0.2 mg/ml) or/and Nano ZSA-51D (100 nM).
1012 **(c)** Quantification (left) and representative flow cytometry plots (right) of $CD69^+$ OT-I $CD8^+$ T
1013 cell activation after co-incubation with differently treated neutrophils for 48 hours (n = 3). ****p
1014 < 0.0001.
1015 **(d)** Quantification (left) and representative flow cytometry plots (right) of OT-I $CD8^+$ T cell
1016 proliferation by CSFE staining after co-incubation with differently treated neutrophils for 48 hours
1017 (n=3). ***p < 0.001, ****p < 0.0001.
1018 **(e)** Bright-field microscopy images of OT-I CD8+ T cells after co-incubation with differently
1019 treated IA ($CD101^-CD14^+$) and MA ($CD101^+CD14^+$) neutrophils for 48 hours. IA ($CD101^-CD14^+$)
1020 and MA ($CD101^+CD14^+$) neutrophils were sorted from bone marrow pretreated overnight with
1021 Nano ZSA-51D (100 nM) with or without OVA.
1022 **(f)** Quantification (left) and representative flow cytometry plots (right) of $CD69^+$ OT-I $CD8^+$ T cell
1023 activation after co-incubation with differently treated IA (CD101-CD14+) and MA
1024 (CD101+CD14+) neutrophils for 48 hours (n=3). ****p < 0.0001.
1025 **(g)** Quantification (left) and representative flow cytometry plots (right) of OT-I $CD8^+$ T cell
1026 proliferation by CSFE staining after co-incubation with differently treated IA (CD101-CD14+)
1027 and MA (CD101+CD14+) neutrophils for 48 hours (n=3). ****p < 0.0001.
1028

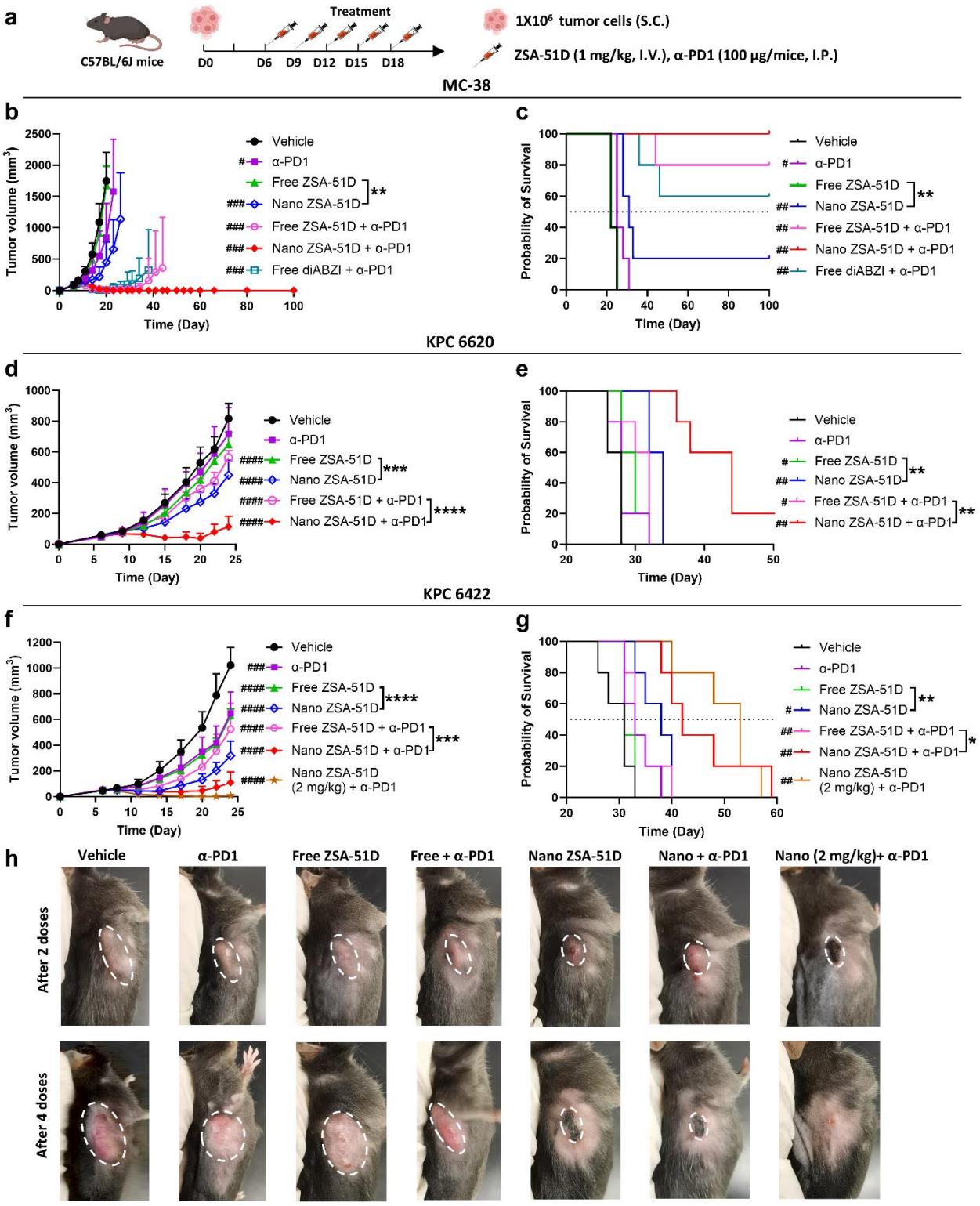

Figure 5. Nano ZSA-51D in combination with α-PD1 achieves potent therapeutic efficacy in colon and pancreatic cancer models.

1032 **(a)** Schematic Illustration of the cancer model establishment in C57BL/6J mice and treatment
1033 regimen in tumor-bearing mice.
1034 **(b-g)** Tumor growth curves (b, d, f) and survival curves (c, e, g) of MC-38 colon (b, c), KPC 6620
1035 (d, e) and KPC 6422 (f, g) pancreatic cancer model following the indicated treatment regimens.
1036 Unless otherwise indicated, ZSA-51D or diABZI was administered at 1 mg/kg (I.V.) and α-PD1 at
1037 100 μg/mouse (I.P.) (n = 5). *$p < 0.05$, **$p < 0.01$, ***$p < 0.001$, ****$p < 0.0001$. #$p < 0.05$, ##p
1038 < 0.01, ###$p < 0.001$, ####$p < 0.0001$ vs. vehicle group.
1039 **(h)** Representative tumor images of the KPC 6422 pancreatic cancer model at 2 and 4 doses post-
1040 treatment. The white dashed line indicates tumor margin.

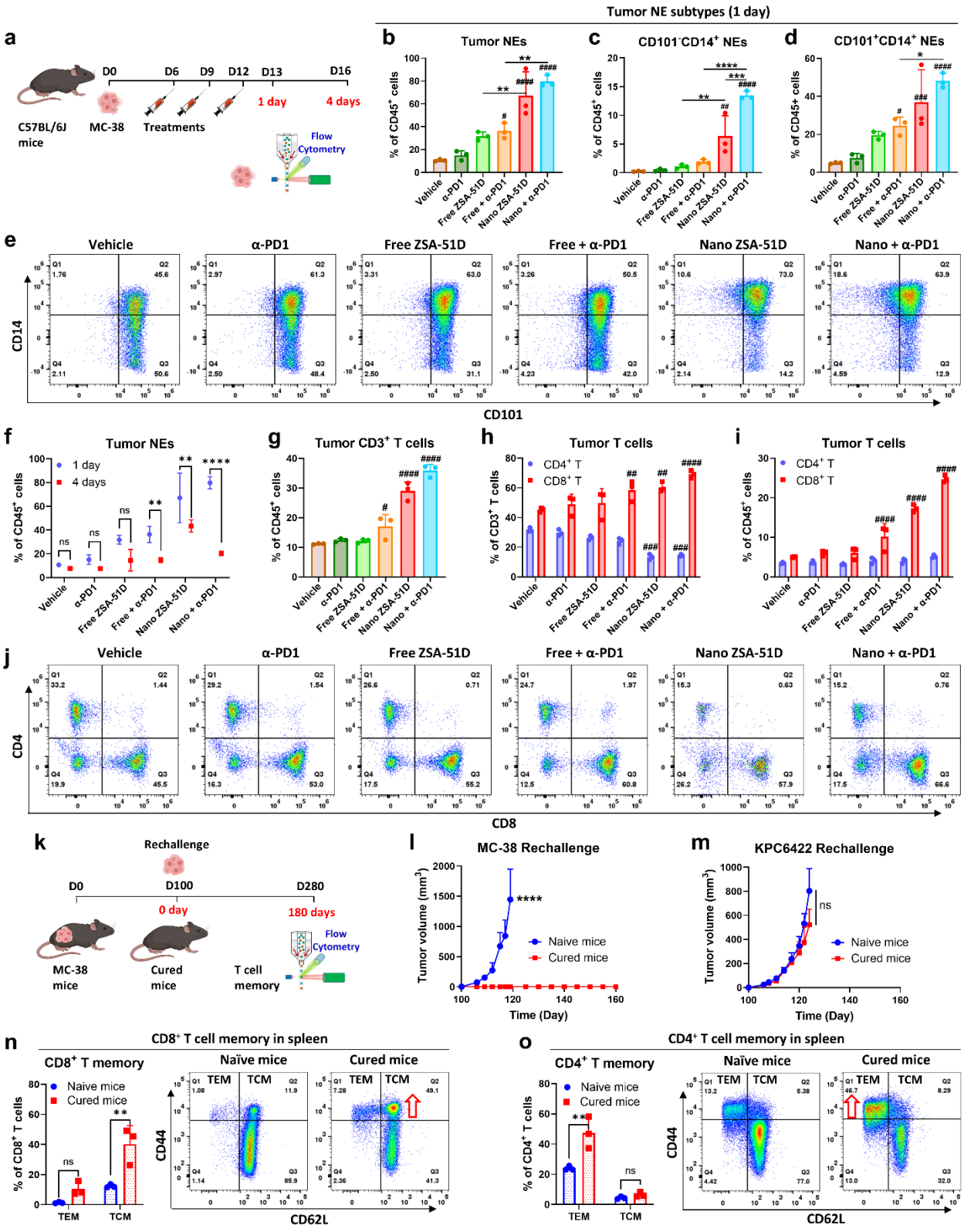

Figure 6. Nano ZSA-51D-induced neutrophil infiltration enhances durable CD8⁺ T cell responses and long-term memory in TME.

(a) Schematic illustrating the treatment schedule and flow cytometry analysis of tumor-infiltrating immune cells in MC-38 tumor-bearing C57BL/6J mice at 1 day and 4 days post-treatment.

(b-d) Quantification of total tumor-infiltrating neutrophils (NEs) (b), $CD101^{-}CD14^{+}$ (c) and $CD101^{+}CD14^{+}$ (d) NEs within $CD45^{+}$ immune cells at 1-day post-treatment (n = 3). *$p < 0.05$, **$p < 0.01$, ***$p < 0.001$, ****$p < 0.0001$; #$p < 0.05$, ##$p < 0.01$, ###$p < 0.001$, ####$p < 0.0001$ vs. vehicle group.

(e) Representative flow cytometry plots of $CD101^{-}CD14^{+}$ and $CD101^{+}CD14^{+}$ neutrophils in MC-38 tumors at 1-day post-treatment.

(f) Quantification and comparison of tumor-infiltrating neutrophils within $CD45^{+}$ immune cells at 1 day and 4 days post-treatment (n = 3). **$p < 0.01$, ****$p < 0.0001$.

(g-i) Quantification of $CD3^{+}$ T cells within $CD45^{+}$ immune cells (g), $CD4^{+}$ and $CD8^{+}$ T cells within $CD3^{+}$ T cells (h) or within $CD45^{+}$ immune cells (i) at 4 days post-treatment (n = 3). #$p < 0.05$, ##$p < 0.01$, ###$p < 0.001$, ####$p < 0.0001$ vs. vehicle group.

(j) Representative flow cytometry plots of tumor-infiltrating $CD4^{+}$ and $CD8^{+}$ T cells within $CD3^{+}$ T cells at 4 days post-treatment.

(k) Schematic of MC-38 tumor cell rechallenge in mice cured with Nano ZSA-51D and α-PD1 combination therapy at 100 days post-treatment. Long-term T cell memory was evaluated by flow cytometry at 180 day post-rechallenge.

(**l, m**) Tumor growth curves following rechallenge with MC-38 (l) or KPC 6422 (m) tumor cell in naïve C57BL/6J mice and cured mice at 100 days post-treatment (n=5). ****$p < 0.0001$; ns, not significant.

(n, o) Quantification (left) and representative flow cytometry plots (right) of $CD8^{+}$ (n) and $CD4^{+}$ (o) effector memory (TEM: $CD62L^{-}CD44^{+}$) and central memory (TCM: $CD62L^{+}CD44^{+}$) T cells in the spleen of naïve C57BL/6J mice and cured mice at 180-day post-rechallenge (n=3). **$p < 0.01$; ns, not significant.